Atmos. Meas. Tech. Discuss., https://doi.org/10.5194/amt-2018-79
Manuscript under review for journal Atmos. Meas. Tech.
Discussion started: 5 April 2018

Atmospheric Measurement Techniques
Open Access
Discussions

A multi-wavelength numerical model in support to quantitative retrievals of aerosol properties from automated-lidar-ceilometers and test applications for AOT and PM10 estimation

Davide Dionisi[1], Francesca Barnaba[1], Henri Diémoz[2], Luca Di Liberto[1], Gian Paolo Gobbi[1]

[1]Istituto di Scienze dell'Atmosfera e del Clima, Consiglio Nazionale delle Ricerche (ISAC-CNR), Roma, Italy
[2]Aosta Valley Regional Environmental Protection Agency (ARPA Valle d'Aosta), Saint-Christophe (Aosta), Italy

Correspondence to: Davide Dionisi (d.dionisi@isac.cnr.it)

Abstract. Knowledge of the height-distribution of aerosol particles is a key factor in the study of climate, air pollution, and meteorological processes. The use of automated lidar-ceilometers (ALC) for the aerosol vertically-resolved characterization has increased in the recent years thanks to their low construction and operation costs, and to their capability in providing continuous, unattended measurements. The quantitative assessment of the aerosol properties from ALC measurements and the relevant assimilation in meteorological forecast models is amongst the main objectives of the EU COST Action TOPROF (Towards Operational ground-based PROFiling with ALCs, doppler lidars and microwave radiometers). Concurrently, the E-PROFILE program of the European Meteorological Services Network (EUMETNET) focuses on the harmonization of ALC measurements and data provision across Europe. Within these frameworks, we implemented a methodology to retrieve key aerosol properties (extinction coefficient, surface area and volume) from lidar and/or ALC measurements. The method is based on results from a large set of aerosol scattering simulations (Mie-theory) performed at UV, visible and near IR wavelengths using a "Monte-Carlo" approach to select the input aerosol microphysical properties. A 'continental aerosol type' is addressed in this study. Based on the model results, we derived mean functional relationships linking the aerosol backscatter coefficients and the above-mentioned variables. Applied in the data inversion of single wavelength lidars/ALCs, these relationships allow quantitative determination of the vertically-resolved aerosols backscatter, extinction, volume and surface area, and in turn of the extinction-to-backscatter ratio (i.e., the lidar-ratio, LR) and of extinction-to-volume conversion factor (c_v) at 355, 532, 1064 nm. These variables provide valuable information for visibility, radiative transfer and air quality applications. This study also includes validation of the model results with real measurements, and test applications of the proposed model-based ALC inversion methodology. In particular, our model simulations were compared to backscatter and extinction coefficients retrieved by Raman lidar systems at different continental sites in Europe operating within the European Aerosol Research LIdar NETwork (EARLINET). This comparison showed good model-measurements agreement, with LR discrepancies below 20%. The model-assisted retrieval of both aerosol extinction and volume was then tested using raw data from three different ALCs systems (CHM15k-Nimbus), operating within the Italian Automated Lidar-ceilometer Network (ALICENET). To this purpose, a one-year-record of the ALCs-derived aerosol optical thickness (AOT) at each site was compared to direct AOT measurements performed by co-located sun-sky photometers. This comparison resulted into an overall AOT agreement within 30% at all sites. At one site, the model-assisted ALC estimation of the aerosol volume and mass (i.e., PM10) in the lowermost 75 m was compared to values measured at the surface-level by co-located in situ instrumentation. This comparison showed rather good agreement too. In particular, the ALC-derived daily-mean mass concentration was found to well reproduce corresponding PM10 values measured by the local Air Quality agency in terms of both temporal variability and

absolute values (mean relative difference around 15%). The good performances of the proposed approach in these preliminary tests suggest it could possibly represent a valid option to extend the capabilities of ALCs at providing quantitative information for operational air quality and meteorological monitoring.

1 Introduction

Due to the impact of atmospheric aerosols on both air quality and climate, substantial efforts have been made to expand our knowledge of their sources, properties and fate. Aerosol particles affect the Earth's radiation budget mainly by two different processes: scattering and absorbing both solar and terrestrial radiation (aerosol direct effect, Haywood and Boucher, 2000) and serving as cloud and ice condensation nuclei (aerosol indirect effect, Lohmann and Feichter, 2005). The complexity of these processes and the extreme spatial and temporal variability of the aerosol sources, physical and chemical properties and atmospheric processing make the quantification of this impact very difficult. Aerosols have also proven detrimental effects on human health (D'Amato et al., 2013, World Health Organization, 2013, Lelieveld et al., 2015). In fact, their concentration (often evaluated in terms of particulate matter mass, or PM) is regulated by specific air quality legislation worldwide. In Europe, the Air Quality Directive 2008/50 defines the 'objectives for ambient air quality designed to avoid, prevent or reduce harmful effects on human health and the environment as a whole' (EC, 2008).

Among the aerosol observational systems, the LIDAR technique has been proved to be the optimal tool to provide range-resolved accurate aerosol data necessary in radiative transfer computations (e.g. Koetz et al., 2006) and is often usefully employed in support to air quality studies (e.g. Menut et al., 1997, He et al., 2012). With a spectrum of different system types (elastic backscatter, Raman, High Spectral Resolution, and multi-wavelength lidars), each with specific pro and cons, this technique allows retrievals of aerosol and cloud optical properties and relevant distribution within the atmospheric column at several ground-based observational sites (Fernald et al., 1972; Klett, 1981; Shipley et al., 1983, Kovalev and Eichinger, 2004, Heese and Wiegner, 2008; Ansmann et al., 2012). Since 2006, the Cloud Aerosol Lidar and Infrared Pathfinder Satellite Observation (CALIPSO) platform (Winker et al. 2003) also provides a unique, global view of aerosol and cloud vertical distributions through space-based observations (at the operating wavelengths of 532 and 1064 nm). Space-borne lidar observations are however affected by some drawbacks, as limited temporal resolution and spatial coverage (the CALIPSO spatial distance between two consecutive ground tracks is about 1000 kilometers and each track has a footprint of 70 m), the contamination of unscreened clouds, and difficulties in quantitatively characterizing the aerosol properties in the lowermost troposphere (Pappalardo et al., 2010). Ground-based lidar networks thus still represent key tools in integrating spaceborne observations to study aerosol properties and 4D distribution. An example of these networks is the European Aerosol Research LIdar NETwork (EARLINET, http://www.earlinet.org/), which, since 2000, provides an extensive collection of ground-based data for the aerosol vertical distribution over Europe (Bösenberg et al., 2003, Pappalardo et al., 2014). The advanced multi-wavelength elastic and Raman lidars employed in this network allows independent retrieval of aerosol extinction (α_a) and backscattering coefficient (β_a) profiles, which are essential information to the assessment of the aerosol radiative effects. Yet, despite their unsurpassed potential of a detailed characterization of aerosol particles, advanced lidar networks such as EARLINET have the unsolved problem of the sparse spatial and temporal sampling. In fact, the typical distance between the EARLINET stations is of the order of several hundreds of kilometers and regular measurements of EARLINET are only performed on selected days of the week (Mondays and Thursdays) and for a few hours (mainly at nighttime, due to low signal-to-noise in daylight). Furthermore, these systems are complicated to be operated, requiring specific expertise, and are therefore unsuitable for operational applications.

Atmos. Meas. Tech. Discuss., https://doi.org/10.5194/amt-2018-79
Manuscript under review for journal Atmos. Meas. Tech.
Discussion started: 5 April 2018

Atmospheric Measurement Techniques Discussions

Nowadays, hundreds of single channel Automated Lidar Ceilometers (ALCs) are in operation over Europe. Although such simple lidar-type instruments were originally designed for cloud base detection only, the recent technological advancements make now these systems reliable and affordable, increasing the interest in using this technology in different aerosol-related sectors (e.g. air quality, aviation security, meteorology, etc.). In particular, recent studies showed that the ALC technology is now mature enough to be used for a quantitative evaluation of the aerosol physical properties in the lower atmosphere (Wiegner, M. and A. Geiß, 2012, Wiegner et al., 2014). The exploitation of the full potential of ALCs in the aerosol remote sensing is a current matter of discussion in the lidar community (e.g. Madonna et al., 2015). In Europe, such evaluation is for example among the main objectives of the EU COST Action ES1303, TOPROF (Towards Operational ground-based PROFiling with ALCs, doppler lidars and microwave radiometers). An effort in this direction is also underway in the framework of E-PROFILE, one of the observation programs of EUMETNET (EUropean METorological services NETwork). In fact, several ALC stations are progressively joining E-PROFILE to develop an operational network to produce and exchange ALC-derived profiles of attenuated backscatter. A recent project funded by the EU LIFE+ program (DIAPASON, Desert-dust Impact on Air quality through model-Predictions and Advanced Sensors ObservatioNs, LIFE+2010 ENV/IT/391) also prototyped and tested an ALC system with an additional depolarization channel capable of discriminating non spherical aerosol types, such as desert dust (Gobbi et al., 2018). Such upgraded ALC systems could further improve the capabilities of the operational aerosol profiling in a near future.

Given the necessity to couple advancement in instrumental technology with tools capable of translating raw data into a robust, quantitative and usable information, this work presents a general methodology to estimate some key aerosol optical and physical properties from ALCs. This is intended to contribute achieving a full exploitation of these systems potential in integrating data collected by more advanced lidar systems/networks. In particular, the aerosol properties addressed in this study are: backscatter ($ß_a$, km^{-1} sr^{-1}), extinction (α_a, km^{-1}), surface area (S_a, cm^{-2}/cm^{-3}) and volume (V_a, cm^{-3}/cm^{-3}), the latter being convertible into aerosol mass (µg/m^3) via assumption on particle density. For this purpose, we developed an aerosol model to perform aerosol scattering simulations and implemented a procedure that, relying on results from this numerical model, derives mean functional relationships linking $ß_a$ to α_a, S_a and V_a, respectively. These are then applied in the ALC inversion and data analysis. A similar approach was applied in past studies for lidar-based investigations of stratospheric (Gobbi, 1995) and tropospheric aerosols (maritime, desert dust and continental type) at visible and UV lidar wavelengths, (Barnaba and Gobbi, 2001, Barnaba and Gobbi, 2004a, hereafter BG01, BG04a, respectively, Barnaba et al., 2004). Here we expand this approach to all the Nd:YAG laser harmonics commonly used by advanced lidars and ALC systems (i.e. 355, 532, 1064 nm wavelengths) and address an 'average-continental' aerosol type, expected to dominate over most of Europe.

This investigation is organized as follows: in Section 2 we describe the aerosol model intended to reproduce clean to moderately polluted continental conditions and the Monte Carlo methodology followed to perform the computations of the corresponding bulk optical and physical properties. Section 3 shows and discusses the results of the numerical model, and presents the model-based mean functional relationships linking the different variables at 355, 532 and 1064 nm. In Section 4 we evaluate both the model simulations capability to reproduce real measurements in continental aerosol conditions, and the capability of the model-based ALC inversion approach to derive quantitative geophysical information. The EARLINET database was used for the first task while tests on the accuracy of the model-based ALC inversion were performed evaluating the ALC-derived aerosol volume and aerosol optical thickness (AOT, i.e. the vertically integrated aerosol extinction). To this purpose we applyied the proposed methodology to three ALC systems operating within the Italian Automated LIdar-CEilometer NETwork (ALICE-NET, www.alice-net.eu). The ALC-derived AOT and aerosol volume (plus mass) were compared respectively to relevant measurements performed by ground-based sun photometers and in situ aerosol instruments (optical counters and PM10 samplers).

Section 5 summarizes the developed approach and main results critically examining strengths and the weaknesses. It also includes discussion on the perspectives of the application of this (or similar) methodology in operational ALC networks

2 The aerosol model

A numerical aerosol model was set up to calculate mean functional relationships between the aerosol backscatter (β_a) and some relevant aerosol properties and namely extinction, surface area and volume (α_a, S_a and V_a, respectively). This is done in a two-step procedure (Figure 1, following an approach similar to that developed by BG01 and BG04a):

1) Generation of a large set (here 20000) of aerosol optical properties by randomly varying, within appropriate ranges, the microphysical parameters describing the aerosol size distribution and composition (blue box in Fig. 1);

2) Based on results at point 1), determination of mean functional relationships linking key variables (grey box in Fig. 1).

Section 2.1 describes rationale and set-up of the first step, the second one being thoroughly discussed in Section 3.

2.1 Selection of the aerosol microphysical parameters

As anticipated, a 'continental' aerosol type was targeted in this study, this being the aerosol type expected to dominate over Europe. Based on a scheme originally proposed by d'Almeida et al. (1991), and on a large set of following observational evidences (e.g. Putaud et al., 2003), in this work its size distribution is described as an external mixture of three size modes. These are (in order of increasing size range): 1) a first ultrafine mode; 2) a second fine mode, mainly composed of water-soluble particles; 3) a third mode of coarse particles.

A three-mode lognormal size distribution described by Eq. (1) is employed to this purpose:

$$n(r) = \frac{dN}{d\log r} = \sum_{i=1}^{3} \frac{N_i}{\sqrt{2\pi}\log\sigma_i} exp\left[-\frac{(\log r - \log r_i)}{2(\log\sigma_i)^2}\right] \quad (1).$$

In Eq. (1), r_{mi}, σ_i and N_i are respectively the modal radius, the width and the particle number density of the i^{th} aerosol mode (i = 1, 2, 3). At each computation, r_{mi} and σ_i as well as m_{r_i} and m_{im_i} values are randomly chosen within a relevant variability range. Values of N_i are conversely obtained by firstly randomly choosing the total number of particles, N_{tot}, to be included in the whole size distribution ($N_{tot} = N_1 + N_2 + N_3$), and then by applying specific rules for the number mixing ratio x_i (N_i/N_{tot}) of each component to this total. To reproduce clean to moderately polluted continental conditions, the value of N_{tot} is made variable between 10^3 and $3*10^4$ cm^3 (e.g. Hess et al., 1998; Putaud et al., 2003). Being the result of different sources/processes, the three modes are also assumed to have a different composition, this being described by each mode real and imaginary refractive indices (m_{r_i} and m_{im_i}, respectively).

1) First Mode

This ultrafine mode is the one more directly simulating fresh, anthropogenic emissions. The number mixing ratio $x_{i=1}$ ($N_{i=1}/N_{tot}$) of this mode is let variable between 10% (rural conditions, Putaud et al. 2003) and 60% (more polluted conditions, Hess et al., 1998). The size range chosen is such to include either nucleation mode particles or Aitken mode particles. To take into account the wide variability of species within this ultrafine mode, from non-absorbing (inorganic)

Atmos. Meas. Tech. Discuss., https://doi.org/10.5194/amt-2018-79
Manuscript under review for journal Atmos. Meas. Tech.
Discussion started: 5 April 2018

Atmospheric Measurement Techniques Discussions

to highly absorbing materials (e.g. black carbon), wide ranges of variability mode for its refractive indexes were chosen (m_r in the range 1.40 - 1.8, m_i in the range 0.01 – 0.47, at λ=355 nm).

2) Second mode

The second mode accounts for 40-90% of N_{tot}. Its composition (m_{r2}, and m_{i2}) is also made highly variable so to include water soluble inorganic and organic particles (Hess et al., 1998; BG04a; Dinar et al. 2008). In this case, m_r is in the range 1.40 - 1.7 and m_i is in the range 0.0001 – 0.01, at λ=355 nm.

3) Third mode

This larger mode is mainly intended to account for soil derived (dust-like) particles that are a primary continental emission. A narrow variability is fixed for its m_r and m_i (1.5 – 1.6 and 0.0001 – 0.01, respectively at 355 nm). The relevant number mixing ratio x_3 (N_3/N_{tot}) is set variable between 0.001% – 0.5 %, this mode contributing most to the total aerosol volume (thus mass) but very little to the total number of particles.

Additionally, and again linked to the different composition, wavelength dependent refractive indexes are also introduced. For the second mode (water-soluble particles) we include an increase with the wavelength of the upper boundary values of m_{i2} and the decrease of m_{r2} at λ =1064 nm as reported by d'Almeida et al. (1991). For the (dust-like) third-mode particles, the upper boundary values of m_{i3} are set to decrease with increasing wavelengths (Gasteiger et al., 2011, Wagner et al., 2012).

The variability range of the different parameters as emerging based on literature data is summarized in Table 1. Based on these datasets, the overall variability range used in this work for each parameter is given in Table 2.

Also note that, for convenience, the aerosol parameters boundaries of Table 2 refer to dry particles and to ground level. However, the effect of a variable RH, its variability with altitude as well as the generally observed decrease of particle number with altitude is also considered in the model. In fact, while first and third modes are assumed to be water insoluble, the second mode is fully hygroscopic. More specifically, the number of particles in each mode, N_i, and RH are both made altitude-dependent through the following equations:

$$N_i(z) = N_i(0) \times \exp\left(\frac{-z}{H_i}\right), \tag{2}$$

$$RH(z) = 70 \times \exp\left(\frac{-z}{5.5\ km}\right) \times (1 + dRH), \tag{3}$$

the altitude z being made variable here between 0 and 5 km. Aerosol humidification is also considered to act on both particle size and refractive indices of the second aerosol mode (e.g., BG1), as:

$$r_{mi\_RH} = r_{mi\_0}\sqrt{\frac{2-0.01RH}{2(1-0.01RH)}}, \tag{4}$$

$$m_{RH} = m_0 + m_0 - m_w \left(\frac{r_{mi\_0}}{r_{mi\_RH}}\right)^3, \tag{5}$$

where $m_i = m_{r\_i} - i \times m_{im\_i}$. To describe the altitude effect, in eq. (2) an exponential decrease with height of the particle number density is assumed. $N_i(0)$ and H_i are the number of particles at the ground and the scale height for each mode, respectively. To rescale the particle number density of the different modes, $H_{i=1=2}$ is set equal to 5.5 km while $H_{i=3}$ (coarse particles) is set to 0.8 Km (Barnaba et al., 2007). In eq. (3), the additional term (1+dRH) is set to allow a further variability of ±60% with respect to the mean RH(z) profile assumed (the value of dRH being randomly chosen between

Atmos. Meas. Tech. Discuss., https://doi.org/10.5194/amt-2018-79
Manuscript under review for journal Atmos. Meas. Tech.
Discussion started: 5 April 2018

-60 and +60). Values of RH greater than 95% are discarded to avoid divergence. In eq. 4 and 5, r_{im_RH} and m_{iRH} are the RH-corrected modal radius and refractive index, respectively; r_{mi0} and m_{i0} are the particle dry modal radius and refractive index, respectively; m_w is the water refractive index (assumed as equal to 1.34 – i7e^{-9}, 1.33 - i1.3e^{-9} 1.33 - i2.9e^{-6} at 355, 532 and1064 nm, respectively). Furthermore, following Barnaba et al. (2007), an increase of the width of the size distribution with altitude (eq. 6) has been introduced for the first and second aerosol mode:

$$\sigma_{1,2}(z) = \sigma_{1,2,z0} \times \exp\left(\frac{z}{30}\right). \tag{6}$$

In fact, Barnaba et al., (2007) showed that this was necessary to better reproduce the observed decrease of the Lidar Ratio (LR) with altitude, and likely related to a broadening of the particle size distribution with aging.

Once the value of each microphysical parameter is randomly selected within its relevant variability range, and once corrections are applied following eqs. (2) – (6), the resulting aerosol size and composition-resolved distribution is used to feed a Mie code (assumption of spherical particles) to compute $ß_a$, α_a, S_a and V_a, (BG01, see also Fig. 1) as:

$$\beta_a = \int Q_{bsc}(r,\lambda,m)\,\pi r^2 \frac{dN_i}{d\log r}\frac{1}{r\ln 10}dr \tag{7}$$

$$\alpha_a = \int Q_{ext}(r,\lambda,m)\,\pi r^2 \frac{dN_i}{d\log r}\frac{1}{r\ln 10}dr \tag{8}$$

$$S_a = 4\pi \int r^2 \frac{dN}{d\log r}\frac{1}{r\ln 10}dr \tag{9}$$

$$V_a = \frac{4}{3}\pi \int r^3 \frac{dN}{d\log r}\frac{1}{r\ln 10}dr, \tag{10}$$

where Q_{bsc} (r, λ, m) and Q_{ext} (r, λ, m) are, respectively, the backscatter and the extinction efficiencies. As mentioned, the computations are made at the three different wavelengths: 355, 532, 1064 nm (i.e., those of Nd:YAG laser harmonics, the most common wavelengths used by ground-based and space-borne aerosol lidars).

Since in our simulations the third aerosol mode is intended to represent dust-like particles, an empirical correction for non-sphericity is finally also applied to the Mie-derived optical properties of this mode. This procedure is based on BG01, which uses the results of Mishchenko et al. (1997) obtained for surface-equivalent mixtures of prolate and oblate spheroids. In particular, the values of α_a and LR_a are corrected as a function of the effective size parameter ($x_{eff} = \pi r/\lambda$) using the different curves reported in Mishchenko et al. (1997) for three different values of the size distributions effective variance v_{eff} (v_{eff} = 0.1, 0.2, 0.4, see equation (13) of Mishchenko et al., 1997 for the definition of v_{eff}).

3 Model simulations results

The 20000 simulations of continental aerosol optical and physical properties derived randomly varying the relevant aerosol size distributions and compositions as described in the previous section are shown in Figure 2. In particular, the results for α_a, S_a and V_a are shown as a function of $ß_a$ in Figure 2a, b, c (blue crosses) referring to λ = 1064 nm. For each variable (A) average values per bin of $ß_a$ and relevant standard deviations (<A> ± dA) are shown as red dots and vertical bars, respectively. Note that 10 equally spaced bins per decade of ß have been considered, and <A> ± dA are only shown for bins containing at least 1% of the total points. Corresponding relative errors (dA/<A>) are depicted in the Figure 2d, e, f. Some tests on the sensitivity of these model results to the variability of the microphysical parameters employed are provided in Appendix B.

Based on these results, at step-two of the procedure (see scheme in Figure 1), we derive aerosol-specific mean relationships linking aerosol extinction, surface area and volume (α_a, S_a and V_a) to its backscatter ($ß_a$). To this purpose, we used a seventh-order polynomial fit in log-log coordinates. These relationships are shown as green lines in Figure 2a, b, c while the relevant fit parameters are reported in Table 3 (λ = 1064 nm, fit parameters related to computations at λ = 355 and 532 nm, being given in Table A1 and Table A2, Appendix A).

The red vertical bars of Figure 2 also highlight the $ß_a$ regions in which, at λ = 1064 nm, the model provides at least 1% of the total points for α_a, S_a and V_a. These are: 10^{-4} - 10^{-1} km^{-1}, 10^{-7} - 10^{-5} cm^2/cm^2 and 10^{-13} - 10^{-10} cm^3/cm^3, respectively. These values correspond to the backscatter range $9\times10^{-5} \leq ß_a \leq 4\times10^{-3}$ km^{-1} sr^{-1}. In terms of aerosol properties variability, the relative errors associated to α_a and V_a show almost no dependence on $ß_a$, with values between 30% and 40%. Conversely, the modeled aerosol surface area exhibits a larger dispersion, with relative error values spanning the range 40% - 70%, and decreasing as $ß_a$ increases.

A key parameter for the inversion of lidar signals is the so-called Lidar Ratio (*LR*), i.e. the ratio between α_a and $ß_a$ (Ansmann et al., 1992). In Figure 3 we show the results in terms of LR vs $ß_a$ for our simulations at λ = 355, 532 and 1064 nm (Figure 3a, b, c, respectively) and relevant dLR/LR values (Figure 3d, e, f, respectively). The color code is the same of that in Fig. 2. Additional horizontal black lines have been inserted representing mean values (solid central lines) of the 'weighted-LR' ± 1 s. d. (dotted side lines), i.e. LR weighted by the number of simulated points in each considered backscatter bin. The 'weighted-LR' values derived at 355, 532 and 1064 nm, are 50.1 ± 17.9 sr, 49.6 ± 16.0 sr and 37.7 ± 12.6 sr, respectively.

Figure 3 also allows showing that the statistically significant regions of simulated backscatter values shifts towards smaller values with increasing λ (e.g. at λ = 355, the $ß_a$ extending regions is 4×10^{-5} - 2×10^{-2} km^{-1} sr^{-1}, whereas, at 532 nm, it ranges between 2×10^{-5} - 1×10^{-2} km^{-1} sr^{-1}).

These results also show a quite different shape of the LR vs $ß_a$ functional relationships (green curves) at different wavelengths is obtained. At 355 and 532 nm the curve is concave, with quite similar LR maxima (54.3 and 53.8 sr at approximately $ß_a = 4\times10^{-4}$ km^{-1} sr^{-1} and 2×10^{-3} km^{-1} sr^{-1}, respectively). At 1064 nm the curve is conversely monotonic, with a flex point at $ß_a$ = 3-4×10^{-4} km^{-1} sr^{-1}. A larger data dispersion also characterizes the results at λ = 355, 532 nm (LR values from <20 to > 90 sr) in comparison to λ = 1064 nm (LR in the range 18 – 80 sr). This translates into relative error differences between UV, VIS and infrared (IR) wavelengths. At 1064, dLR/LR slightly decreases for increasing backscatter, with values around 35%. At the shorter wavelengths, it increases as a function of $ß_a$, with a large (>40%) relative error for values of $ß_a > 2\times10^{-3}$ km^{-1} sr^{-1}.

To insert our results into a more general context, we compared the derived, model-based weighted-LR values to some LR data reported in the literature (Table 4). In particular, we selected some of the works using the aerosol model developed to invert the Calipso lidar data (Omar et al., 2009). This latter considers six different aerosol sub-types: clean continental (CC), clean marine (CM), dust (D), polluted continental (PC), polluted dust (PD), and smoke (S). Our model-derived LR at 532 nm falls in the middle of the range (35-70 sr) fixed by the Calipso CC and PC aerosol classes. The work by Papaggianopoulos et al. (2016), in which the LR values are adjusted accordingly to EARLINET observations, reports a LR range at 532 nm of 47-62 sr. At the same wavelength, the aerosol range defined by the LIVAS climatology (LIdar climatology of Vertical Aerosol Structure for space-based lidar simulation studies, Amiridis et al., 2015), is 54-64 sr. In both cases, our model seems to be closer to the LR values of CC aerosol type, which is compatible to our intention to simulate clean-to-moderately polluted continental aerosol type. At 532 nm, our LR value is also reasonably in between the CC and PC LR values derived by Omar et al. (2009), but again closer to the CC LR value. The very small decrease of LR values between 532 and 355 nm estimated by LIVAS for the CC aerosol is also consistent with our results. Similarly, our model predicts a lower mean LR in the near IR with respect to the green, in agreement with results of Amiridis et al. (2015) in CC conditions and not to those in polluted conditions. Table 4 also includes the continental aerosol LR values estimated in the work of Düsing et al. (2018) through comparison between airborne in situ and ground-based lidar measurements. Our model is in good agreement with their LR values at 355 and 532 nm. At 1064 nm, the algorithm developed by Düsing et al. (2018) provided a value of LR around 15 sr. On the other hand, in the same study the authors found that, rather, a value of LR = 30 sr gives the better accord between their Mie and lidar-based α_a, this value being closer to our model-derived one at 1064 nm (LR =37.7). The difference between these two values is explained by the authors to be probably due to the estimation of the aerosol particle number size distribution, a critical parameter for a reliable modeling of aerosol particle backscattering.

4 Evaluation of the model performances and potential of its application

In this section, we evaluate the capability of the model results to reproduce 'real' aerosol conditions and explore the potential of the proposed model-based inversion to exploit the ALC measurements potential in producing quantitative geophysical information. In particular:

- In Section 4.1 we compare our simulations to real observations of backscatter and extinction coefficients made by different EARLINET Raman lidars (Bösenberg et al., 2001, Pappalardo et al., 2014).

- In Section 4.2, our model results are used to invert measurements acquired by some ALCs systems of the Italian 'Automated LIdar-CEilometer NETwork' (ALICE-NET, www.alice-net.eu). ALICE-NET is composed of several ALCs systems (Nimbus CHM15k by Lufft) located across Italy and run by Italian research institutions and environmental agencies. Here we use data from some of these systems to derive the aerosol optical and physical properties (e.g. the aerosol optical thickness, AOT, and the aerosol volume and mass).

4.1 Comparison of the modelled aerosol optical properties to EARLINET measurements

EARLINET Raman stations perform coordinated measurements three times per week following a schedule established in 2000 (Bösenberg et al., 2003).Overall, the EARLINET database includes the following categories: 'climatology', 'CALIPSO', 'Saharan dust', 'volcanic eruptions', 'diurnal cycles', 'cirrus', and 'others' (forest fires, photo smog, rural or urban, and stratosphere). To be compared to our results, we used EARLNET β_a and α_a coefficients at 355 nm and at 532 nm within the quality assured (QA) 'climatology' category (Pappalardo et al., 2014). Note however that additional data filtering was necessary to screen out unreliable values. In particular, we only selected those EARLINET QA data further satisfying the following criteria:

- β_a and α_a coefficients evaluated independently, i.e. using only the Raman method (Ansmann et al., 1992);
- β_a and $\alpha_a > 0$;
- LR < 100;
- Relative errors on β_a and α_a < 30%.
- Desert dust free data (i.e. we removed from our 'comparison data set' all the dates within the 'climatology' category that were also included in the EARLINET 'Saharan dust' category).

We then selected those sites in Europe expected to be mostly impacted by 'continental' aerosols and having the largest dataset (e.g., more than 100 points) at 355 and 532 nm. Overall, 5 sites satisfied these conditions (Table 5), and namely Madrid (Spain), Potenza and Lecce (Italy), Leipzig and Hamburg (Germany).

Atmos. Meas. Tech. Discuss., https://doi.org/10.5194/amt-2018-79
Manuscript under review for journal Atmos. Meas. Tech.
Discussion started: 5 April 2018

Atmospheric Measurement Techniques Discussions

For the EARLINET Raman stations selected, Figure 4 depicts the results of the model-measurements comparison in terms of LR vs β_a at λ=355 nm. The colored area represents the model-simulated data range, the color code indicating the absolute number of simulated values (i.e. counts) in each β_a -LR pair. The EARLINET-measured values are reported as black open circles. Note that, being the model simulations performed over an altitude range 0-5 km (see Section 2.1) only those values simulated in the altitude range (Δz) covered by the measurements at each EARLINET station was taken into account. Figure 4 shows that the model results well encompass the measured LR vs β_a data, with few measurements outside the modeled range (most of the exceptions are found for Potenza). The highest number density of simulated data also well fits the observations, with the exception of Hamburg (Figure 4a), which however has the poorer database in terms of number (it isn't an EARLINET station any longer).

In Figure 5 the previous results at λ=355 nm are converted in terms of 'mean' LR per bin of β_a for both model (blue) and observations (red). Note that only β_a bins containing at least 1% of the total modeled data were considered. This view shows that there is a general good agreement between the modeled and the measured LR values, and in their variation with β_a. Some major deviations are found for Potenza and will be discussed in the following (the corresponding results at λ=532 nm including Madrid in place of Hamburg is given in Appendix C, Figure C1). In quantitative terms, the model-measurements accordance shown in Figure 5 was evaluated computing mean LR relative differences, i.e. ($[(LR_{mod}- LR_{meas})/ LR_{meas}]*100$), at both λ = 355 and 532 nm. These values are reported in Table 6 for each considered EARLINET station, together with the measurements-based mean LR in each observational site (computed weighting the number of observations per β_a spaced bins).

Results in Figure 5 and Table 6 also give some hints on the capability of the aerosol type assumed (and its admitted range of variability) to reproduce 'real' continental aerosol conditions in different sites across Europe. In fact, the four continental sites selected with our criteria are still expected to be impacted by different continental-like aerosol types.

- A good agreement between the model and the observations in terms of LR mean values is found for Hamburg (Figure 5a), with mean LR differences of the order of 5% (Table 6). Still, the measured LR values have a high variability and their distribution is positioned towards high values of β_a (1×10^{-3} to 4×10^{-3} km^{-1} sr^{-1}). This could be due to the presence of different aerosols type as slightly polluted marine and polluted aerosol (Matthias and Bösenberg, 2002).

- A good accord for Leipzig (Fig. 5c) also indicates that this site is mostly dominated by 'pure' continental particles. In fact, the distribution of observed LR points in Fig. 4, which covers β_a values ranging from 2×10^{-4} to 3×10^{-3} km^{-1} sr^{-1}, is well centered to the modeled simulations highest density (counts > 40). Table 6 shows that at both wavelengths mean discrepancies with LR measurements keep well below 10%.

The highest differences in Fig. 5 are found in some southern Europe EARLINET sites:

- In Lecce (Fig. 5b), the best agreement between model and observations is found for the lowest values of β_a (between 9×10^{-4} to 1×10^{-3} km^{-1} sr^{-1}). Also, the increase from 10% to 18% in the discrepancies at 355 and 532 nm indicates some model problems in correctly reproducing the spectral variability of the optical properties, suggesting some mismatch between modeled and real aerosol sizes in this site (see discussion below).

- In Potenza (Fig. 5d), a significant difference between the mean LR curves emerges for β_a values > 6×10^{-4} km^{-1} sr^{-1} with observed LR values lower than those simulated here.

Atmos. Meas. Tech. Discuss., https://doi.org/10.5194/amt-2018-79
Manuscript under review for journal Atmos. Meas. Tech.
Discussion started: 5 April 2018

These discrepancies could be due to the influence of marine aerosols at both stations (De Tomasi et al., 2006, Mona et al., 2006, Madonna et al., 2011), which is expected to produce lower LR values for high values of $ß_a$ (e.g. BG01). In fact, Madrid shows better performances, with dLR/LR comparable to those in Leipzig.

To provide some insight into the reasons of the model-measurements differences at LC and PO sites, some model sensitivity tests have been performed and are reported in Appendix D. In particular, for Lecce, reducing the variability range of N_{tot} (from 500 - 10000 cm^{-3} to 500 - 5000 cm^{-3} at ground) permits to better fit the observed LR vs β_a behavior at 355 nm. This indicates that LC is affected by cleaner continental aerosol type conditions. The simulation done for Potenza shows that an additional increase of the variability range of the coarse mode radius is needed to reproduce the observed decrease of LR for increasing backscatter (Figure 5d). This suggests a presence of larger coarse particles than those assumed in such clean continental environment (APPENDIX B), this is compatible with the suspect of marine air contamination although at this stage we are not able to exclude additional contamination of coarse particle of soil origin.

Overall, mean LR differences between our continental model and data at selected European sites keep lower than 20% (Table 5), this indicating our general model reasonably well reproduces the clean-to-moderately polluted continental aerosol conditions we intended to simulate.

4.2 Model results application to Nimbus CHM15-k ALC measurements

To test and validate the model-based inversion methodology, we used the derived functional relationships to invert and analyze the measurements acquired by some ALICENET ALCs (Lufft CHM15k systems). These instruments are a biaxial ceilometers that emit laser pulses at 1064 nm (Nd:YAG-laser, class M1) with a typical pulse energy of 8 µJ and a pulse repetition rate of about 6500 Hz. The instruments have a specified range of 15 km and full overlap at around 1500 m (Heese et al., 2010). The manufacturer provides the overlap correction functions (*O(z)*) for each system. As shown recently by Wiegner and Geiß (2012) and Wiegner et al. (2014), a promising strategy to retrieve the aerosol backscatter coefficient from ALC measurement is adopting the forward solution of the Klett inversion algorithm (Klett 1985). This solution requires a known calibration constant of the system (i.e. absolute calibration) and an assumption on the LR. The advantage with respect to the backward solution is that calibration is not affected by the low SNR in the upper troposphere and it is needed occasionally. Furthermore, starting close to the surface, the data retrieval allows resolving aerosol layers in the boundary layer even if their optical depth is high. The forward solution of the Klett inversion algorithm is thus adopted here, the detailed algorithm procedure being described in Wiegner and Geiß (2012) (equations 1 – 3). In particular, in this study we use the forward solution, with a daily calibration constant provided by the backward approach (Rayleigh calibration) applied to nighttime and cloud-free signal averaged over 1 or 2 hours at 75 m height resolutions.

4.2.1 Model-based retrieval of aerosol optical properties

To isolate the aerosol contribution to the ceilometer signals, the contribution of molecular backscatter and extinction coefficients to the raw ALC data are calculated from climatological monthly air density profiles. Inversion of the aerosol properties, $\alpha_a(z)$ and $\beta_a(z)$, is then performed using an iterative technique since we need to correct the backscatter signal at each altitude z for extinction losses. The iterative procedure is stopped when convergence in the integrated aerosol backscatter ($IAB=\Sigma_0^{zcal}\beta a(z)$) is reached (e.g. BG01). At each step, aerosol extinction is derived using the functional relationship $\alpha_a = \alpha_a(\beta_a)$ of Table 3. The ALC-derived AOT is obtained vertically integrating $\alpha_a(z)$ from

Atmos. Meas. Tech. Discuss., https://doi.org/10.5194/amt-2018-79
Manuscript under review for journal Atmos. Meas. Tech.
Discussion started: 5 April 2018

the surface up to a fixed height z_{AOT}, above which the aerosol contribution is assumed to be negligible. An example of the outcome of this retrieval methodology is depicted in Figure 6. It shows the time-height contour plot (24h, 0 - 6 km) of the α_a retrieved at 1064 nm during a whole day of measurements (June 26, 2016) performed by the ALICENET system of Aosta San Chrisophe (Northern Italy). Time and altitude resolutions are 1 min and 15 m, respectively. Note that ALC data are cloud-screened using the cloud mask of the Lufft firmware. Superimposed to the extinction contour, we include the ALC-derived AOT values at 1064 nm (pink curve, with a temporal resolution of 5 min) and the AOT values from a co-located sun-sky radiometer (a Prede POM-02 system, orange circles) extrapolated at 1064 nm using the Angström exponent derived fitting AOT values at all the radiometer wavelengths. This example illustrates the very good performances of our model-assisted inversion scheme, and the capability of this approach to extend to nighttime the radiometer observations.

To evaluate the performances of our model-assisted retrieval of $\alpha_a(z)$ over a statistically significant dataset, the same approach illustrated in Figure 6 was applied to a wider record. In particular, we used Nimbus CHM-15k ALC datasets from three different ALICENET sites: Aosta Saint Christophe (ASC, 45.8°N, 7.4°E 570 m a.s.l.), San Pietro Capofiume (SPC, 44°39N, 11°37E, 10 m a.s.l.) and Rome Tor Vergata (RTV, 41.88°N, 12.68°E, 100 m a.s.l.). The location of the three systems is shown in Figure 7a (red circles), while some information on system types and site characteristics is given in Table 6. The data analyzed here were collected during the following periods: April 2015 – June 2017, June 2012 – June 2013 and February 2014 – September 2015, for ASC, SPC and RTV, respectively. Only AOT values between 0.01 and 0.2 at 1064 nm were considered. Overall a total of 1237, 268, 850 AOT pairs were analyzed.

Although CHM-15k data are already corrected for the *O(z)* function provided by the manufacturer, the variation of the ALC internal temperature can lead to *O(z)* differences up to 45% in the first 300 m above ground (Hervo et al., 2016). For this reason, in our analyses the lowest valid altitude of the CHM-15k for both the SPC and RTV systems was fixed to be about 400 m. A linear fit of the first two valid ALC points is then used to extrapolate $\alpha_a(z)$ down to the ground (z_0). Conversely, due to the optimal characterization of *O(z)* provided by Lufft for the CHM-15k system installed at ASC, values at z_0 at this site are not those extrapolated but those actually measured. The maximum altitude of aerosol extinction vertical integration to derive the AOT, z_{AOT}, was selected as the first height above 4000 m where the range corrected signal (RCS) has a signal to noise ratio (SNR) < 1.

The validation dataset used includes AOT measurements collected by sunphotometers co-located to the ALCs: an AERONET Cimel CE 318-2 sun-photometer operational at RTV site (https://aeronet.gsfc.nasa.gov), and two SKYNET Prede sun-sky radiometers at ASC and SPC sites (POM-02L and POM-02, respectively, www.euroskyrad.net). All these passive sensors are co-located with the CHM-15k systems.

Results of the long-term AOT comparison are summarized in Figure 7 and Table 7. For each site under investigation, Figure 7 shows the histograms of the AOT differences between the hourly-mean coincident AOTs as derived by the ALCs and measured by the photometers (red curve). To evaluate the advantage of our approach with respect to more standard lidar inversions, we also computed AOT differences using two fixed-LR values. In particular, we used LR = 52 sr (i.e. the value suggested by the E-profile network, black lines) and LR = 38 sr (i.e. the weighted mean LR value coming out from our model, see Section 3, blue lines).

Figure 7 shows that the best agreement is found at ASC. The distribution of AOT difference has a maximum around 0 for each of the three inversions schemes, with very low dispersion. The full width at half maximum, FWHM, is in fact around 0.015 and approximately 55% of the data are included in the interval -0.01 – 0.01, which is even within the error

Atmos. Meas. Tech. Discuss., https://doi.org/10.5194/amt-2018-79
Manuscript under review for journal Atmos. Meas. Tech.
Discussion started: 5 April 2018

Atmospheric Measurement Techniques
Open Access
Discussions

of photometric measurement. For SPC and RTV, the red and blue histograms are peaked around 0, whereas the black ones have the maxima at around 0.01-0.02 and 0.02-0.03 for SPC and RTV, respectively. These two sites have higher dispersion (FWHM = 0.03 and approximately 30% of the data are included in the interval -0.01 – 0.01 for the red and blue histograms at both sites), which is probably due to the different aerosol load affecting the different ALICENET stations. As pointed out by the low value of the average AOT (<AOT> = 0.027) computed at ASC for the analyzed dataset, low pollution levels generally characterize this site, with some exceptions due to wind-driven aerosol transport from the nearby Po valley (Diémoz et al,, this issue). On the contrary, RTV (<AOT> = 0.044) and, especially, SPC in the Po Valley (<AOT> = 0.076) are characterized by higher aerosol content and pollution levels, which explains the larger histogram dispersions. Note that the high frequency of fog events in winter markedly reduces the number of analyzed AOT pairs at SPC site. Furthermore, note that desert dust affected days were removed from both SPC and RTV datasets.

Table 8 summarizes the long-term performances of the model-based procedure in deriving quantitative AOT from the ALC systems at the three investigated sites. It includes values of the average differences between the ALC-derived and sunphotometers-measured AOT (both bias, < dAOT >, and absolute difference <|dAOT|>, with their standard deviations) using both the proposed model-based approach and the two fixed-LR inversions. For SPC and RTV sites, this test shows that the best ALC–photometer accordance is reached when employing either the model-based or the fixed LR=38 sr inversion schemes. In fact, these two approaches have similar performances in terms of mean dAOT values (<|dAOT|> = 0.11, 0.13 and 0.13, 0.14 for SPC and RTV, respectively), mean percent error (<|dAOT|> /<AOT> = 0.16, 0.19 and 0.31, 0.33) and a very low mean relative bias (<dAOT>/<AOT> = -0.04, 0.05 and 0.09, 0.11). On the other hand, the fixed LR=52 sr retrieval produces an overestimation of AOT in both SPC and RTV (<dAOT>/<AOT> = 0.33 and 0.44) with larger discrepancies between retrieved and observed AOTs (<|dAOT|> = 0.021 and 0.0026, <|dAOT|>/<AOT> = 0.38 and 0.49). For the ASC site, due to the low aerosol content, the differences among the inversion schemes are negligible.

Overall, for the three sites, these results show a very good performance of the model-based approach with similar behavior of the retrieval with a fixed LR of 38 sr, while a fixed LR value of 52 sr produces a clear overestimation of the AOT at SPC and RTV. As different sites have different, and not known, characteristic LR values, these results highlight the potential of the developed approach to derive quite accurate β_a and α_a coefficients without the need to choose and fix an a-priori LR value.

4.2.2 Model-based retrieval of aerosol volume (and mass)

In this section we provide examples of the applicability of the proposed approach to derive air-quality relevant parameters. In particular, we use the model results to derive the aerosol volume from ALC measurements and compare it to measurements of aerosol volume performed by two different optical particle counters (OPCs) in two dates: 29^{th} December 2016 and 5^{th} September 2017. For the case of the 29^{th} December 2016, a TSI Optical Particle Sizer (OPS) 3330 was employed. This instrument has 16 channels that can be programmed to provide the number concentration at different (and logarithmically spaced) size ranges within the interval 0.3 - 10 µm. Further details can be found in the TSI manual (2011). For the case of the 5^{th} September 2017, the Fidas®200s OPC was used. This spectrometer is able to retrieve high-resolution particle spectra (size measurements between 0.15 and 27 µm, with 32 channels/decade, Pletscher et al., 2016).

For both these dates, Figure 8 shows the time (x-axis, 24h) vs. height (left y-axis) contour plots of the ALC-based retrieval of the aerosol volume concentration (cm^3/cm^3). The OPC-derived aerosol volume concentration measured at ground-level is reported as a function of time (x-axis) on the right y-axis (grey curve). The corresponding ALC-derived volume concentration (integrating the ALC data between 0 and 75 m) is shown by a pink curve (same right y-axis). Daily mean volume concentration values derived by OPCs and by ALC are also plotted (grey cross and pink triangle, respectively).

The OPC-to-ALC comparison is certainly affected by intrinsic factors, as differences on the atmospheric layer sampled (at ground and integrated between 0 and 75 m, for OPC and ALC, respectively) and on the probing methods (in-situ and remote sensing, dried air sampled by OPC and ambient conditions sampled by the ALC). Furthermore, as mentioned in Section 4.2.1, a major critical issue of ALC retrievals at low layers is the correction for the overlap function, which needs to be experimentally characterized and verified for each instrument.

These issues are visible in the given example of Figure 8. In fact, in the upper panel, the agreement between ALC and TSI aerosol V_a values is good between 0 and 7 UTC. In the following hours both instruments register an increase of the aerosol volume, although with some discrepancies in absolute values. Starting from 18 UTC, ALC derives an aerosol volume concentration higher than the OPC one by a factor of 3-3.5. This disagreement could be related to both the presence/arrival of small particles (<0.3 μm) not measured by the optical counter (see for example Diemoz et al., 2018), or to aerosol hygroscopic effects (increase of volume associated to hygroscopic growth seen by ALC but not by the OPC which dries the air samples). The lower panel shows a good agreement between the ALC-derived and the Fidas OPC V_a values, in particular until 04 UTC and after 16 UTC. Some differences emerge around 07 UTC and between 11 and 15 UTC, where the ALC volume is lower by a factor of 2 compared to the in situ Fidas V_a values. The smaller minimum detectable size of the Fidas OPC instrument is likely the reason for the better accord between ALC and OPC V_a values.

Even with the mentioned limitations, results in Fig. 8 well show the potential of the developed method in providing sound values of aerosol volume, and hence, mass.

To give a further example in this direction, the model–assisted retrievals were also used over a longer time period to derive daily-mean aerosol mass concentrations (PM10), a measurement typical of air quality stations. To this purpose, and similarly to the previous example, the daily mean aerosol volume in San Pietro Capofiume was derived for the period June-July 2012 using our functional relationships $V_a = V_a(\beta_a)$, and then converted into mass using specific aerosol densities (ρ_a). Results obtained using the ALC data of SPC for the mentioned period are shown in Figure 9. This reports the daily average PM10 concentration measured in situ at SPC by the Italian Regional Environmental Protection Agency (ARPA, red solid curve) and the model-assisted, ALC-derived daily mass concentration obtained assuming both a fixed particle density $\rho_a = 2$ μg/m^3 (blue dotted curve), and a range of it between 1.5-2.5 μg/m^3 (shaded area).

In particular, the daily-mean ALC-derived mass concentrations are estimated in two steps: 1) estimation of hourly mass values for the selected height; 2) computation of the daily values through the median of the hourly values. To guarantee a good daily representativeness, the second step is applied only to those days in which at least 50% of the hourly values is available in all the following temporal periods: 00 - 05 UTC, 06 - 11 UTC, 12 - 17 UTC, 18 - 23 UTC. Note that, due to the uncertainties associated to the $O(z)$ in the first hundreds of meters (see previous section), the selected height used to estimate ALC mass concentration is 225 m. This difference is not expected to impact much the comparison to ground-level PM10 in the considered period of the year (i.e. June and July), which is characterized by a strong convection (e.g. Barnaba et al, 2010). This is confirmed by the good agreement between the ALC-derived and the ARPA PM10 values (Fig. 9). In fact, mean and relative differences between the two series are: <dPM10> = 2.8 ± 6.5 μg/m^3, i.e. of about 15% (<(dPM10/PM10)> = 0.15 ± 0.27).

As a last added value of the outcome from model-based results, we derive here and provide in Table 9 extinction-to-volume conversion factors, $c_v = V_a/\alpha_a$ (e.g., Ansmann et al., 2010) at three different wavelengths (355, 532 1064 nm), and compare these to similar outcomes from other studies. To our knowledge, values of continental particles c_v at the same three wavelengths are only available in Mamouri and Ansmann (2017). Note that c_v, is also proportional, through the particle density ρ_a, to the inverse of the so-called 'mass-to-extinctions efficiency' (MEE, i.e. $\alpha_a/(V_{a*}\rho_a)$) a parameter important in several aerosol-related applications (e.g. the estimation of particulate matter mass from satellite AOT or in modules of global circulation and chemical transport models to compute radiative forcing effects of aerosols (Hand and Malm, 2007). For convenience, model-derived MEE values are also included in Table 9.

5 Summary and Discussion

Thanks to their low construction/operation costs and to their capability at providing continuous, unattended measurements, the use of automated-lidar-ceilometers (ALCs) for aerosol characterization has increased in the recent years. Several numerical approaches were recently proposed to estimate the aerosol vertical profile either using ceilometer measurement only or coupling these with ancillary measurements (e.g., Stachlewska et al., 2010; Flentje et al., 2010; Wiegner et al., 2012; Wiegner et al., 2014; Cazorla et al., 2017, Román et al., 2018).

This work proposes a methodology to retrieve key aerosol properties (as extinction coefficient, surface area and volume, thus mass) from lidar/ALC measurements using, as ancillary information to drive the retrievals, the results from a specifically developed aerosol numerical model. In particular, a "Monte-Carlo" approach is used to simulate a large set (20000) of aerosol microphysical properties intended to reproduce clean-to-moderately polluted continental conditions, i.e., those expected to dominate over Europe. Based on the assumption of particle sphericity (Mie theory), relevant computations of aerosol physical (surface area and volume, S_a and V_a) and optical (backscattering and extinction coefficients, β_a and α_a) properties were performed at the three commonly used lidar wavelengths (i.e., at the Nd:YAG laser harmonics 355, 532, 1064 nm). Fitting procedures of the 20,000 data-pairs obtained for each variable were then used to derive mean functional relationships linking β_a to α_a, S_a and V_a, respectively. The relative errors associated to these mean relationships were found to be between 30% and 40% for β_a vs α_a and β_a vs V_a, respectively, while β_a vs S_a exhibits a larger dispersion (relative error from 40% to 70%). The model results also allowed deriving the lidar ratio (LR) dependence on β_a at 355, 532 and 1064 nm and a mean, 'weighted-LR' values (50.1 ± 17.9 sr, 49.6 ± 16.0 sr and 37.7 ± 12.6 sr, at 355, 532 and 1064 nm respectively). Availability in literature of LR values at 1064 nm are scarce and its monotonic increase with β_a found in this work (Figure 3) suggests that the use of a fixed LR value for the inversion of ALC signals should be done with caution and carefully evaluated case by case. A similar, non monotonic behavior characterize the shapes of LR vs β_a curve at 355 and 532 nm.

To test the reliability of our model results: 1) numerical computations were compared to 'real' lidar measurements, and 2) the model-assisted retrievals of aerosol optical (AOT) and physical (V_a, PM10) properties by real ALC systems were compared to corresponding measurements performed by co-located, independent instrumentation.

In particular, in task 1) our simulations were compared to backscatter and extinction coefficients at 532 and 355 nm independently retrieved by advanced Raman lidar systems operating at different EARLINET sites in Europe (namely Hamburg and Leipzig in Germany, Madrid in Spain, Lecce and Potenza in Italy). The model simulations were found to well match the observations (Figures 4, 5 and C1). Mean discrepancies between model and measurement-based LR

Atmos. Meas. Tech. Discuss., https://doi.org/10.5194/amt-2018-79
Manuscript under review for journal Atmos. Meas. Tech.
Discussion started: 5 April 2018

Atmospheric Measurement Techniques
Discussions

were found to be lower than 20%, suggesting a good capability of the assumed aerosol model (and admitted range of variability) to represent 'real' continental aerosol conditions in different sites across Europe. Some differences emerged for Italian sites, likely affected by the influence of marine aerosols leading to lower LR values for high values of β_a.

For task 2) we applied the proposed model-based inversion to different ALC systems (Lufft CHM-15k), part of the Italian ALICENET network. In particular, the hourly-mean, vertically-integrated aerosol extinction (i.e., the AOT) derived by three ALC systems of Aosta San Cristophe (ASC), San Pietro Capofiume (SPC) and Rome Tor Vergata (RTV, Figure 7) was compared to corresponding measurements of co-located sun-photometers. ALC-sun photometer agreement was found to be within 30%. Tests on the use of fixed LR were also performed to investigate the advantage of the proposed approach with respect to more standard ones. To this purpose, we used the (1064 nm) fixed-LR value suggested by the E-profile Program and the 'weighted mean' coming out from our model (52 sr and 38 sr, respectively). While for the ASC site, negligible differences were found among the three retrieval schemes, for both SPC and RTV sites the best ALC – sun photometer accordance is reached when employing the model-based or the fixed LR=38 sr inversion schemes, with a mean error around 16-19 % and 31-33 % for SPC and RTV, respectively. Applying the fixed LR value of 52 sr produces an overestimation of the AOTs, with a mean relative bias equal to 33 % and 44 % at SPC and RTV, respectively. This suggests that, at 1064 nm, the LR value for continental aerosol is lower than the one assumed by E-Profile procedure.

As a second test in task 2, values of aerosol volume (and mass) derived using the model-assisted ALC retrieval were compared to in situ aerosol measurements performed by OPCs and PM10 analyzers. A continuous, two-months comparison (June – July 2012) between daily average aerosol mass concentration as derived by ALC (lowest altitudes) and measured in situ at SPC, showed a mean relative difference around 15%.

Overall, the main advantage of the proposed approach is the possibility to operationally (i.e. h24) derive aerosol optical properties (β_a, α_a, S_a and V_a and associated uncertainties) without ancillary data information and no-need to use a fixed, a-priori chosen LR in the ALC inversion. It could, therefore, represent a valid option to extend the capabilities of ALCs at providing important information for operational air quality and meteorological monitoring. Moreover, this methodology could be used to temporally and spatially integrate the information coming from more advanced lidar networks (for example, the Raman channel cannot be used in daylight conditions).

Main limitation is that the method is dependent on the considered aerosol type and can, accordingly, reproduce 'mean' aerosol type conditions but it is not adequate to characterize some 'specific aerosol conditions' affecting a given site.

In this respect, it is worth mentioning that this drawback could be partially overcome when the implementation of a depolarization channel in ALCs (as tested in the DIAPASON Project, Gobbi et al., 2018) will be operative and consolidated. In fact, the information coming from the additional channel could be used to force the retrieval to different model schemes (e.g. switching from 'no dust' to 'dust' schemes conditions) in the same vertical profile. This will enhance the capabilities of ALCs to operatively estimate and characterize the aerosol optical properties (e.g. Gasteiger and Freudenthaler, 2014).

Acknowledgements

This work was partly supported by the European Commission Life+ Project "DIAPASON" (LIFE+2010 ENV/IT/391). The study also contributes to the activities of the EU COST Action TOPROF (ES1303). The authors acknowledge EARLINET for providing aerosol lidar profiles through its website (http://access.earlinet.org/) and the EARLINET publishing group 2000-2010 (https://doi.org/10.1594/WDCC/EN_all_measurements_2000-2010). We thank the

EARLINET PIs Ulla Wandinger (Leibniz Institute for Tropospheric Research, Leipzig, Germany), Manuel Pujadas (Centro de Investigaciones Energéticas, Medioambientales y Tecnológicas, Department of Environment, Madrid, Spain), Maria Rita Perrone (Department of Mathematics and Physics, Universita' del Salento, Italy) and Aldo Amodeo (Istituto di Metodologie per l'Analisi Ambientale, CNR-IMAA, Italy) and their staff for establishing, maintaining and running the EARLINET instruments at Leipzig (LE), Madrid (MA), Lecce (LE) and Potenza (PO), respectively. The authors also thank Angelo Lupi, Mauro Mazzola, and Vito Vitale (ISAC-CNR) for the management of the PREDE POM-02L Sun-sky radiometer measurements at San Pietro Capofiume (SPC). AOT data analysis for San Pietro Capofiume and Aosta San Christophe was performed as part of a cooperative activity with the SKYNET network. We acknowledge the AERONET team for the processing of the Rome-Tor Vergata data used in this research effort.

Data availability

AERONET Rome-Tor Vergata sun photometer AOT data were downloaded from the AERONET web page (AERONET, 2017). SKYNET sun photometer AOT data were downloaded from the SKYNET webpage (SKYNET, 2017). EARLINET backscattering and extinction coefficients were downloaded from the EARLINET webpage (EARLINET, 2018). ALICENET ALC raw data are available upon request at alicenet@isac.cnr.it.

References

AERONET: AERONET aerosol data base, available at: http:// aeronet.gsfc.nasa.gov/, last access: 20 September 2017.

Amiridis, V., Marinou, E., Tsekeri, A., Wandinger, U., Schwarz, A., Giannakaki, E., Mamouri, R., Kokkalis, P., Binietoglou, I., Solomos, S., Herekakis, T., Kazadzis, S., Gerasopoulos, E., Proestakis, E., Kottas, M., Balis, D., Papayannis, A., Kontoes, C., Kourtidis, K., Papagiannopoulos, N., Mona, L., Pappalardo, G., Le Rille, O., and Ansmann, A.: LIVAS: a 3-D multi-wavelength aerosol/cloud database based on CALIPSO and EARLINET, Atmos. Chem. Phys., 15, 7127-7153, https://doi.org/10.5194/acp-15-7127-2015, 2015.

Ansmann, A., Wandinger, U., Riebesell, M., Weitkamp, C., and Michaelis, W.: Independent measurement of extinction and backscatter profiles in cirrus clouds by using a combined Raman elastic-backscatter lidar, Appl. Optics, 31, 7113–7131, 1992.

Ansmann, A., Tesche, M., Seifert, P., Groß, S., Freudenthaler, V., Apituley, A., Wilson, K. M., Serikov, I., Linné, H., Heinold, B., Hiebsch, A., Schnell, F., Schmidt, J., Mattis, I., Wandinger, U., and Wiegner, M.: Ash and fine-mode particle mass profiles from EARLINET-AERONET observations over central Europe after the eruptions of the Eyjafjallajökull volcano in 2010, J. Geophys. Res., 116, D00U02, doi:10.1029/2010JD015567, 2011a.

Ansmann, A., Petzold, A., Kandler, K., Tegen, I., Wendisch, M., Müller, D., Weinzierl, B., Müller, T., and Heintzenberg, J.: Saharan mineral dust experiments SAMUM-1 and SAMUM-2: What have we learned? Tellus B, 63, 403–429, doi:10.1111/j.1600- 0889.2011.00555.x, 2011b.

Ansmann, A., Seifert, P., Tesche, M., and Wandinger, U.: Profiling of fine and coarse particle mass: case studies of Saharan dust and Eyjafjallajökull/Grimsvötn volcanic plumes, Atmos. Chem. Phys., 12, 9399–9415, doi:10.5194/acp-12-9399-2012, 2012.

Barnaba, F., and Gobbi, G. P.: Lidar estimation of tropospheric aerosol extinction, surface area and volume: Maritime and desert-dust cases, *J. Geophys. Res.*, **106-D3**, 3005–3018, 2001.

Barnaba, F., and Gobbi, G. P.: Modeling the aerosol extinction versus backscatter relationship for lidar applications: maritime and continental conditions, *J. Atmos. Ocean. Technol.*, **21**, 428–442, 2004a.

Barnaba, F. and Gobbi, G. P.: Aerosol seasonal variability over the Mediterranean region and relative impact of maritime, continental and Saharan dust particles over the basin from MODIS data in the year 2001, Atmos. Chem. Phys., 4, 2367–2391, doi:10.5194/acp-4-2367-2004, 2004b.

Barnaba, F., De Tomasi, F., Gobbi, G. P., Perrone, M. R., Tafuro A., Extinction versus backscatter relationships for lidar applications at 351 nm: maritime and desert aerosol simulations and comparison with observations, Atmospheric Research, 70, 229-259, doi: 10.1016/j.atmosres.2004.02.001, 2004.

Barnaba, F., Tafuro, A. M., De Tomasi, F., and Perrone, M. R.: Observed and simulated vertically resolved optical properties of continental aerosols over southeastern Italy: A closure study, J.Geophys. Res., 112, D10203, doi:10.1029/2006JD007926, 2007.

Barnaba, F., Putaud, J. P., Gruening, C., dell'Acqua, A., and Dos Santos, S.: Annual cycle in co-located in situ, total-column, and height-resolved aerosol observations in the Po Valley (Italy): Implications for ground-level particulate matter mass concentration estimation from remote sensing, J. Geophys. Res., 115, D19209, doi:10.1029/2009JD013002, 2010.

Atmos. Meas. Tech. Discuss., https://doi.org/10.5194/amt-2018-79
Manuscript under review for journal Atmos. Meas. Tech.
Discussion started: 5 April 2018

Atmospheric Measurement Techniques Discussions

Barreto, Á., Cuevas, E., Granados-Muñoz, M.-J., Alados-Arboledas, L., Romero, P. M., Gröbner, J., Kouremeti, N., Almansa, A. F., Stone, T., Toledano, C., Román, R., Sorokin, M., Holben, B., Canini, M., and Yela, M.: The new sun-sky-lunar Cimel CE318-T multiband photometer – a comprehensive performance evaluation, Atmos. Meas. Tech., 9, 631-654, https://doi.org/10.5194/amt-9-631-2016, 2016.

Bösenberg, J., Ansmann, A., Baldasano, J. M., Balis, D., Böckmann, C., Calpini, B., Chaikovsky, A., Flamant, P., Hagard, A., Mitev, V., Papayannis, A., Pelon, J., Resendes, D., Schneider, J., Spinelli, N., Trickl, T., Vaughan, G., Visconti, G., and Wiegner, M.: EARLINET: a European Aerosol Research Lidar Network, in: Advances in Laser Remote Sensing, edited by: Dabas, A., Loth, C., and Pelon, J., Ecole polytechnique, Palaiseau Cedex, France, 155–158, 2001.

Bösenberg, J., Matthias, V., Amodeo, A., Amoiridis, V., Ansmann, A., Baldasano, J. M., Balin, I., Balis, D., Böckmann, C., Boselli, A., Carlsson, G., Chaikovsky, A., Chourdakis, G., Comerón, A., De Tomasi, F., Eixmann, R., Freudenthaler, V., Giehl, H., Grigorov, I., Hågård, A., Iarlori, M., Kirsche, A., Kolarov, G., Komguem, L., Kreipl, S., Kumpf, W., Larchevêque, G., Linné, H., Matthey, R., Mattis, I., Mekler, A., Mironova, I., Mitev, V., Mona, L., Müller, D., Music, S., Nickovic, S., Pandolfi, M., Papayannis, A., Pappalardo, G., Pelon, J., Pérez, C., Perrone, R. M., Persson, R., Resendes, D. P., Rizi, V., Rocadenbosch, F., Rodrigues, A., Sauvage, L., Schneidenbach, L., Schumacher, R., Shcherbakov, V., Simeonov, V., Sobolewski, P., Spinelli, N., Stachlewska, I., Stoyanov, D., Trickl, T., Tsaknakis, G., Vaughan, G., Wandinger, U., Wang, X., Wiegner, M., Zavrtanik, M., and Zerefos. C.: EARLINET: A European Aerosol Research Lidar Network to Establish an Aerosol Climatology, Max-Planck-Institut Report No. 348, 2003.

Boucher, O., Randall, D., Artaxo, P., Bretherton, C., Feingold, G., Forster, P., Kerminen, V.-M., Kondo, Y., Liao, H., Lohmann, U., Rasch, P., Satheesh, S. K., Sherwood, S., Stevens, B., and Zhang, X.Y.: Clouds and Aerosols. In: Climate Change 2013: The Physical Science Basis. Contribution of Working Group I to the Fifth Assessment Report of the Intergovernmental Panel on Climate Change [Stocker, T.F., D. Qin, G.-K. Plattner, M. Tignor, S.K. Allen, J. Boschung, A. Nauels, Y. Xia, V. Bex and P.M. Midgley (eds.)]. Cambridge University Press, Cambridge, United Kingdom and New York, NY, USA, pp. 571–658, doi:10.1017/CBO9781107415324.016, 2013.

Cazorla, A., Casquero-Vera, J. A., Román, R., Guerrero-Rascado, J. L., Toledano, C., Cachorro, V. E., Orza, J. A. G., Cancillo, M. L., Serrano, A., Titos, G., Pandolfi, M., Alastuey, A., Hanrieder, N., and Alados-Arboledas, L.: Near-real-time processing of a ceilometer network assisted with sun-photometer data: monitoring a dust outbreak over the Iberian Peninsula, Atmos. Chem. Phys., 17, 11861-11876, https://doi.org/10.5194/acp-17-11861-2017, 2017

d'Almeida, G. A., Koepke, P., and Shettle, E. P.: Atmospheric Aerosol-Global Climatology and Radiative Characteristics, A. Deepack Hampton, VA. 561 pp., 1991.

D'Amato, G., Baena-Cagnani, C. E., Cecchi, L., Annesi-Maesano, I., Nunes, C., Ansotegui, I., D'Amato, M., Licciardi, G., Sofia, M., and Canonica, W. G.: Climate change, air pollution and extreme events leading to increasing prevalence of allergic respiratory diseases, Multidisciplinary Respiratory Medicine, 8(1), 12. http://doi.org/10.1186/2049-6958-8-12, 2013.

De Tomasi, F., Tafuro, A. M., and Perrone, M. R.: Height and seasonal dependence of aerosol optical properties over south-east Italy, J. Geophys. Res., 111, D10203, doi:10.1029/2005JD006779, 2006.

Diémoz, H., Barnaba, F., Magri, T., Pession, G., Dionisi, D., Brunier, A., Lupato, G. Pignet, M., Pittavino, S., Proment, P., Tarricone, C., Tombolato, I. K. F., Vaccari, S., Gibellino, M. C., Zublena, M., Campanelli, M., Della Ceca, L.,

Atmos. Meas. Tech. Discuss., https://doi.org/10.5194/amt-2018-79
Manuscript under review for journal Atmos. Meas. Tech.
Discussion started: 5 April 2018

Atmospheric Measurement Techniques
Discussions

Hervo, M., Di Liberto, L., Ferrero, L., and Gobbi, G. P.: Impact of Po Valley aerosol pollution over the northwestern Alps, Atmos. Chem. Phys., in preparation, 2018.

Davide Dionisi, Claudia Tarricone, Ivan K. F. Tombolato, Stefania Vaccari, Maria Cristina Gibellino, Manuela Zublena, Monica Campanelli, Lara Della Ceca, Maxime Hervo, Luca Di Liberto, Luca Ferrero, and Gian Paolo Gobbi

Dinar, E., Abo Riziq, A., Spindler, C., Erlick, C., Kiss, G., and Rudich, Y.: The complex refractive index of atmospheric and model humic□like substances (HULIS) retrieved by a cavity ring down aerosol spectrometer (CRD-AS), Faraday Discuss., 137, 279–295, 2008.

Düsing, S., Wehner, B., Seifert, P., Ansmann, A., Baars, H., Ditas, F., Henning, S., Ma, N., Poulain, L., Siebert, H., Wiedensohler, A., and Macke, A.: Helicopter-borne observations of the continental background aerosol in combination with remote sensing and ground-based measurements, Atmos. Chem. Phys., 18, 1263-1290, https://doi.org/10.5194/acp-18-1263-2018, 2018.

EARLINET: EARLINET data base, available at: http://www.earlinet.org, last access: 11 January 2018.

EC, 2008. Directive 2008/50/EC of the European Parliament and of the Council of 21 May 2008 on Ambient Air Quality and Cleaner Air for Europe. OJ L 152, 11.6.2008, pp. 1e44. http://eur-lex.europa.eu/LexUriServ/LexUriServ.do?uri¼OJ: L:2008:152:0001:0044:EN:PDF, 2008.

Fernald, F. G., Herman, B. M., and Reagan J. A.: Determination of Aerosol Height Distributions by Lidar, J. Appl. Meteor., 11, 482–489, doi:10.1175/1520-0450(1972)011h0482:DOAHDBi2.0.CO;2, 1972.

Flentje, H., Claude, H., Elste, T., Gilge, S., Köhler, U., PlassDülmer, C., Steinbrecht, W., Thomas, W., Werner, A., and Fricke, W.: The Eyjafjallajökull eruption in April 2010 – detection of volcanic plume using in-situ measurements, ozone sondes and lidar-ceilometer profiles, Atmos. Chem. Phys., 10, 10085–10092, doi:10.5194/acp-10-10085-2010, 2010.

Gasteiger, J., Groß, S., Freudenthaler, V., and Wiegner, M.: Volcanic ash from Iceland over Munich: mass concentration retrieved from ground-based remote sensing measurements, Atmos. Chem. Phys., 11, 2209–2223, doi:10.5194/acp-11-2209- 2011, 2011.

Gasteiger, J. and Freudenthaler, V.: Benefit of depolarization ratio at λ = 1064 nm for the retrieval of the aerosol microphysics from lidar measurements, Atmos. Meas. Tech., 7, 3773-3781, https://doi.org/10.5194/amt-7-3773-2014, 2014.

Gobbi, G. P.: Lidar estimation of stratospheric aerosol properties: Surface, volume, and extinction to backscatter ratio. J. Geophys. Res., 100, 11 219–11 235, 1995.

Gobbi, G. P., Barnaba, F. Di Liberto, L., Bolignano, A., Lucarelli, F., Nava, S., Perrino, C., Pietrodangelo, A., Basar, S., Costabile, F., Dionisi, D., Rizza, U., Canepari, S., Sozzi, R., Morelli, M., Manigrasso, M., Drewnick, R. F., Struckmeier, C., Poenitz, K., and Wille, H.: An integrated view of Saharan Dust Advections to Italy and the Central Mediterranean: Main Outcomes of the 'DIAPASON' Project, submitted to Atmospheric Environment, 2018.

Haarig, M., Engelmann, R., Ansmann, A., Veselovskii, I., Whiteman, D. N., and Althausen, D.: 1064 nm rotational Raman lidar for particle extinction and lidar-ratio profiling: cirrus case study, Atmos. Meas. Tech., 9, 4269–4278, https://doi.org/10.5194/amt9-4269-2016, 2016.

Atmos. Meas. Tech. Discuss., https://doi.org/10.5194/amt-2018-79
Manuscript under review for journal Atmos. Meas. Tech.
Discussion started: 5 April 2018

Atmospheric Measurement Techniques
Open Access
EGU
Discussions

Hand, J. L., and Malm,W. C.: Review of aerosol mass scattering efficiencies from ground-based measurements since 1990, J. Geophys. Res.,112, D16203, doi:10.1029/2007JD008484, 2007.

Hanel, G.: The properties of atmospheric aerosol particles as function of the relative humidity at thermodynamic equilibrium with the surrounding moist air, Adv. Geophys., 19, 73–188, 1976

Haywood, J. M., and Boucher, O.: Estimates of the direct and indirect radiative forcing due to tropospheric aerosols: A review, Rev. Geophys., 38, 513–543, 2000.

He, T.-Y., Stanič, S., Gao, F., Bergant, K., Veberič, D., Song, X.-Q., and Dolžan, A.: Tracking of urban aerosols using combined LIDAR-based remote sensing and ground-based measurements, Atmos. Meas. Tech., 5, 891-900, https://doi.org/10.5194/amt-5-891-2012, 2012.

Heese, B., and Wiegner, M.: Vertical aerosol profiles from Raman polarization lidar observations during the dry season AMMA field campaign, J. Geophys. Res.- Atmos., 113, doi:10.1029/2007JD009487, 2008.

Heese, B., Flentje, H., Althausen, D., Ansmann, A., and Frey, S.: Ceilometer lidar comparison: backscatter coefficient retrieval and signal-to-noise ratio determination, Atmos. Meas. Tech., 3, 1763–1770, doi:10.5194/amt-3-1763-2010, 2010.

Hervo, M., Poltera, Y., and Haefele, A.: An empirical method to correct for temperature-dependent variations in the overlap function of CHM15k ceilometers, Atmos. Meas. Tech., 9, 2947-2959, https://doi.org/10.5194/amt-9-2947-2016, 2016.

Hess, M., Koepke, P., and Schult, I.: Optical properties of aerosols and clouds: The software package OPAC. Bull. Amer. Meteor. Soc., 79, 831–844, 1998.

Holben, B. N., Eck, T. F., Slutsker, I., Tanré, D., Buis, J. P., Setzer, A., Vermote, E.; Reagan, J. A.; Kaufman, Y. J., Nakajima, T., Lavenu, F., Jankowiak, I., and Smirnov, A.: AERONET - A federated instrument network and data archive for aerosol characterization. *Remote Sensing of Environment*, *66*(1), 1-16. DOI: 10.1016/S0034-4257(98)00031-5, 1998.

Klett, J. D.: Stable analytical inversion solution for processing lidar returns, *Appl. Optics*, **20**, 211–220, 1981.

Klett, J. D.: Lidar inversion with variable backscatter/extinction ratios, Appl. Opt., 24, 1638–1643, doi:10.1364/AO.24.001638, 1985.

Koetz, B.; Sun, G.; Morsdorf, F.; Ranson, K.J.; Kneubuhler, M.; Itten, K.; Allgower, B., "Inversion of Combined Radiative Transfer Models for Imaging Spectrometer and LIDAR Data," *2006 IEEE* International Symposium on Geoscience and Remote Sensing, Denver, CO, pp. 395-398. doi: 10.1109/IGARSS.2006.106, 2006.

Kovalev, V. A., and Eichinger , W. E.: Elastic Lidar. Theory, Practice, and Analysis Methods, 615 pp., John Wiley & Sons, Weinheim, Germany, 2004.

Lelieveld, J.; Evans, J.S.; Fnais, M.; Giannadaki, D.; Pozzer, A., The contribution of outdoor air pollution sources to premature mortality on a global scale, Nature, 525, 367–371, 2015.

Levy, R. C., Remer, L. A., and Dubovik, O.: Global aerosol optical properties and application to Moderate Resolution Imaging Spectroradiometer aerosol retrieval over land *J. Geophys. Res., Vol. 112, D13210, doi: 10.1029/2006JD007815,* 2007.

Atmos. Meas. Tech. Discuss., https://doi.org/10.5194/amt-2018-79
Manuscript under review for journal Atmos. Meas. Tech.
Discussion started: 5 April 2018

Lewandowski, P. A., Eichinger, W. E., Holder, H., Prueger, J., Wang, J., and Kleinman, L. I.: Vertical distribution of aerosols in the vicinity of Mexico City during MILAGRO-2006 Campaign, Atmos. Chem. Phys., 10, 1017-1030, https://doi.org/10.5194/acp-10-1017-2010, 2010.

Lohmann, U., and Feichter, J.: Global indirect aerosol effects: A review, Atmos. Chem. Phys., 5, 715–737, 2005.

Lopatin, A., Dubovik, O., Chaikovsky, A., Goloub, P., Lapyonok, T., Tanré, D., and Litvinov, P.: Enhancement of aerosol characterization using synergy of lidar and sun-photometer coincident observations: the GARRLiC algorithm, Atmos. Meas. Tech., 6, 2065-2088, doi:10.5194/amt-6-2065-2013, 2013.

Madonna, F., Amodeo, A., Boselli, A., Cornacchia, C., Cuomo, V., D'Amico, G., Giunta, A., Mona, L., and Pappalardo, G.: CIAO: the CNR-IMAA advanced observatory for atmospheric research, Atmos. Meas. Tech., 4, 1191–1208, doi:10.5194/amt4-1191-2011, 2011.

Madonna, F., Amato, F., Vande Hey, J., and Pappalardo, G.: Ceilometer aerosol profiling versus Raman lidar in the frame of the INTERACT campaign of ACTRIS, Atmos. Meas. Tech., 8, 2207-2223, https://doi.org/10.5194/amt-8-2207-2015, 2015.

Mamali, D., Marinou, E., Sciare, J., Pikridas, M., Kokkalis, P., Kottas, M., Binietoglou, I., Tsekeri, A., Keleshis, C., Engelmann, R., Baars, H., Ansmann, A., Amiridis, V., Russchenberg, H., and Biskos, G.: Vertical profiles of aerosol mass concentrations observed during dust events by unmanned airborne in-situ and remote sensing instruments, Atmos. Meas. Tech. Discuss., https://doi.org/10.5194/amt-2017-422, in review, 2018.

Mamouri, R. E. and Ansmann, A.: Fine and coarse dust separation with polarization lidar, Atmospheric Measurement Techniques, 7, 3717– 5 3735, 2014.

Mamouri, R.-E. and Ansmann, A.: Potential of polarization lidar to provide profiles of CCN-and INP-relevant aerosol parameters, Atmospheric Chemistry and Physics, 16, 5905–5931, 2016.

Matthias, V., and Bösenberg, J.: Aerosol climatology for the planetary boundary layer derived from regular lidar measurements, *Atmos. Res.*, **63**, 221–245, 2002.

Menut, L., Flamant, C., Pelon, J., Valentin, R., Flamant, P. H., Dupont, E., and Carissimo, B.: Study of the boundary layer structure over the Paris agglomeration as observed during the ECLAP Experiment, in: Advances in atmospheric remote sensing with lidar, edited by: Ansmann, A., Neuber, R., Rairoux, P., and Wandinger, U., Springer, Berlin, 15–18, 1997.

Mishchenko, M.I., Travis, L.D., Kahn, R.A., and West, R.A.: Modeling phase functions for dustlike tropospheric aerosols using a mixture of randomly oriented polydisperse spheroids. *J. Geophys. Res.*, **102**, 16831-16847, doi:10.1029/96JD02110, 1997.

Mona, L., Amodeo, A., Pandolfi, M., and Pappalardo, G.: Saharan dust intrusions in the Mediterranean area: Three years of Raman lidar measurements, J. Geophys. Res., 111, D16203, doi:10.1029/2005JD006569, 2006.

Omar, A. H., Winker, D. M., Kittaka, C., Vaughan, M. A., Liu, Z. Y., Hu, Y. X., Trepte, C. R., Rogers, R. R., Ferrare, R. A., Lee, K. P., Kuehn, R. E., and Hostetler, C. A.: The CALIPSO automated aerosol classification and lidar ratio selection algorithm, J. Atmos. Ocean. Tech., 26, 1994–2014, doi:10.1175/2009jtecha1231.1, 2009.

Papagiannopoulos, N., Mona, L., Alados-Arboledas, L., Amiridis, V., Baars, H., Binietoglou, I., Bortoli, D., D'Amico, G., Giunta, A., Guerrero-Rascado, J. L., Schwarz, A., Pereira, S., Spinelli, N., Wandinger, U., Wang, X., and

Pappalardo, G.: CALIPSO climatological products: evaluation and suggestions from EARLINET, Atmos. Chem. Phys., 16, 2341-2357, https://doi.org/10.5194/acp-16-2341-2016, 2016.

Pappalardo, G., Wandinger, U., Mona, L., Hiebsch, A., Mattis, I., Amodeo, A., Ansmann, A., Seifert, P., Linne, H., Apituley, A., Alados Arboledas, L., Balis, D., Chaikovsky, A., D'Amico, G., De Tomasi, F., Freudenthaler, V., Giannakaki, E., Giunta, A., Grigorov, I., Iarlori, M., Madonna, F., Mamouri, R.-E., Nasti, L., Papayannis, A., Pietruczuk, A., Pujadas, M., Rizi, V., Rocadenbosch, F., Russo, F., Schnell, F., Spinelli, N.,Wang, X., and Wiegner, M.: EARLINET correlative measurements for CALIPSO: first intercomparison results, J. Geophys. Res., 115, D00H19, doi:10.1029/2009JD012147, 2010.

Pappalardo, G., Amodeo, A., Apituley, A., Comeron, A., Freudenthaler, V., Linné, H., Ansmann, A., Bösenberg, J., D'Amico, G., Mattis, I., Mona, L., Wandinger, U., Amiridis, V., Alados-Arboledas, L., Nicolae, D., and Wiegner, M.: EARLINET: towards an advanced sustainable European aerosol lidar network, Atmos. Meas. Tech., 7, 2389-2409, https://doi.org/10.5194/amt-7-2389-2014, 2014.

Perrone, M. R., De Tomasi, F., and Gobbi, G. P.: Vertically resolved aerosol properties by multi-wavelength lidar measurements, Atmos. Chem. Phys., 14, 1185-1204, doi:10.5194/acp-14-1185-2014, 2014.

Pletscher, K., Weiss, M., and Moelter, L.: Simultaneous determination of PM fractions, particle number and particle size distribution in high time resolution applying one and the same optical measurement technique, Gefahrst. Reinhalt. L., 76, 425-436, http://www.gefahrstoffe.de/gest/article.php?data[article_id]=86622, 2016.

Putaud, J.-P., Van Dingenen, R., Baltensperger, U., Brüggemann, E., Charron, A., Facchini, M. C., Decesari, S., et al.: A European aerosol phenomenology; physical and chemical characteristics of particulate matter at kerbside, urban, rural and background sites in Europe, European Commission, Report nr. EUR 20411 EN, 2003.

R. Román, Benavent-Oltra, J. A., Casquero-Vera, J. A., Lopatin, A., Cazorla, A., Lyamani, H., Denjean, C., Fuertes, D. Pérez-Ramírez, D., Torres, B., Toledano, C., Dubovik, O., Cachorro, V. E., de Frutos, A. M., Olmo, F. J., and Alados-Arboledas, L.: Retrieval of aerosol profiles combining sunphotometer and ceilometer measurements in GRASP code, Atm. Res., Vol. 204, 15 May 2018, 161-177, https://doi.org/10.1016/j.atmosres.2018.01.021, 2018.

Shipley, S. T. Tracy, D. H., Eloranta, E. W., Tauger, J. T., Sroga, J. T., Roesler, F. L., and Weinman J. A.: High spectral resolution lidar to measure optical scattering properties of atmospheric aerosols. 1: Theory and instrumentation, Appl. Opt. 22, 3716–3724, 1983.

Sicard, M., Guerrero-Rascado, J. L., Navas-Guzman, F., Preißler, J., ´ Molero, F., Tomas, S., Bravo-Aranda, J. A., Comer ´ on, A., Roca- ´ denbosch, F., Wagner, F., Pujadas, M., and Alados-Arboledas, L.: Monitoring of the Eyjafjallajokull volcanic aerosol plume over ¨ the Iberian Peninsula by means of four EARLINET lidar stations, Atmos. Chem. Phys., 12, 3115–3130, doi:10.5194/acp-12-3115- 2012, 2012.

SKYNET: SKYNET data base, available at: http://www.skynet-isdc.org/index.php, last access: 15 September 2017.

TSI, Model 3330 optical particle sizer spectrometer operation and service manual, P/N 6004403, Revision E, April 2011

Wagner, R., Ajtai, T., Kandler, K., Lieke, K., Linke, C., Müller, T., Schnaiter, M., and Vragel, M.: Complex refractive indices of Saharan dust samples at visible and near UV wavelengths: a laboratory study, Atmos. Chem. Phys., 12, 2491-2512, doi:10.5194/acp-12-2491-2012, 2012.

Whitby, K. T.: Physical Characteristics of Sulfur Aerosols. Atmos. Environ. 12:135-159, 1978.

Wiegner, M. and Geiß, A.: Aerosol profiling with the Jenoptik ALC CHM15kx, Atmos. Meas. Tech., 5, 1953–1964, doi:10.5194/amt-5-1953-2012, 2012.

Wiegner, M., Madonna, F., Binietoglou, I., Forkel, R., Gasteiger, J., Geiß, A., Pappalardo, G., Schäfer, K., and Thomas, W.: What is the benefit of ceilometers for aerosol remote sensing? An answer from EARLINET, Atmos. Meas. Tech., 7, 1979-1997, https://doi.org/10.5194/amt-7-1979-2014, 2014.

Winker, D. M., Pelon, J. R., and McCormick, M. P.: The CALIPSO mission: Spaceborne lidar for observation of aerosol and clouds, SPIE Proc. Ser., vol. 4893, Soc. Photo-Opt. Instrum. Eng., Bellingham, Washington, 2003.

World Health Organization, Review of Evidence on Health Aspects of Air Pollution REVIHAAP Project, Technical Report, World Health Organization: Copenhagen, Denmark, 2013.

Table 1. Aerosol parameter values as reported in literature for continental-type aerosols.

Reference	*r_1 (μm)* *σ_1*	*r_2 (μm)* *σ_2*	*r_3 (μm)* *σ_3*	*N_1/N_{tot}* *(%)*	*N_2/N_{tot}* *(%)*	*N_3/N_{tot}* *(%)*	*m_{r1},* *m_{im1}*	*m_{r2}* *m_{im2}*	*m_{r3}* *m_{im3}*	*N_{tot}* *(cm^{-3})*	Aerosol type
Whitby (1978)[1]	0.008 1.6	0.034 2.1	0.46 2.2	0.56	0.44	4×10^{-4}	-	-	-	1800	Clean continental
D'Almeida et al. (1991)[2]	0.012 2.0	0.029 2.24	0.471 2.51	0.06	0.94	2×10^{-6}	1.75 0.44	1.53 0.012	1.53 0.008	20000	Average continental
Hess et al. (1998)[2]	0.012 2.0	0.021 2.24	0.471 2.51	0.56	0.44	0.3×10^{-4}	1.75 0.44	1.53 0.012	1.53 0.008	15300	Average continental
Barnaba and Gobbi (2004a)[1]	0.007-0.012 1.7 – 2.0	0.021 – 0.077 2.03 – 2.24	0.403 – 0.5 2.11 – 2.24	6.1– 54.2	45.8 – 93.9	$(2 – 26.1) \times 10^{-4}$	1.25–2.00 0.07–1.00	1.53 6×10^{-3}	1.53 8×10^{-3}	10^3 - 10^4	
Omar et al. (2009)[1]	-	0.093-0.10 1.53-1.61	0.68-0.76 1.9-2.1	-	0.999-1	$(0.02\text{-}3) \times 10^{-4}$	-	1.38-1.40 $(0.1 – 6.3) \times 10^{-3}$	1.40-1.46 $(3.4\text{-}6.3) \times 10^{-3}$	-	Clean and polluted continental
Levy et al. (2007)[2]	0.018 2.0	0.005 2.97	0.5 2.97	1	1×10^{-7}	1×10^{-13}	1.75 0.44	1.53 6×10^{-3}	1.53 8×10^{-3}	-	
Barnaba et al. (2007)[1]	-	0.05-0.1 1.35-1.70	0.4-0.5 1.5-2.0	-	0.98-0.99	0.01-0.02	-	1.35-1.55 $(2.5 – 20) \times 10^{-3}$	1.53-1.6 $(1.0 – 80) \times 10^{-4}$	$1\text{-}3 \times 10^3$	Continental - coastal
Amiridis et al. (2015)[1]	-	0.03-0.9 1.6-2.2	0.47-0.69 1.9-2.5	-	1	$(4 – 8) \times 10^{-7}$	-	1.42-1.45 $(2.3 – 6) \times 10^{-3}$	1.45-1.53 $(2.3 – 6) \times 10^{-3}$	-	Clean and polluted continental

[1]The refractive index are for λ=532 nm.

[2]The refractive index are for λ=550 nm.

Atmos. Meas. Tech. Discuss., https://doi.org/10.5194/amt-2018-79
Manuscript under review for journal Atmos. Meas. Tech.
Discussion started: 5 April 2018

Table 2. Variability Ranges used in this study. Values refer to ground and dry conditions (see text for details).

Parameter	Mode I	Mode II	Mode III
r_m (μm)	0.005 - 0.03	0.03 - 0.1	0.3 - 0.5
σ	1.35 – 1.7	1.35 – 1.7	1.5 – 2.4
N_i/N_{tot} (%)	10 - 60	40 - 90	0.01 – 0.5
m_r (355 nm)	1.40 – 1.80	1.40 – 1.70	1.50 – 1.60
(532 nm)	1.40 – 1.80	1.40 – 1.70	1.50 – 1.60
1064 (nm)	1.42 – 1.82	1.37 – 1.66	1.50 – 1.60
m_{im} (355 nm)	1×10^{-2} – 0.47	1×10^{-4} – 0.010	1×10^{-4} – 0.02
(532 nm)	9×10^{-3} – 0.44	1.2×10^{-4} – 0.012	1×10^{-4} – 0.01
1064 (nm)	9×10^{-3} – 0.44	1.5×10^{-4} – 0.015	1×10^{-4} – 0.005
N_{tot} (cm^{-3})	500 – 10000		

Atmos. Meas. Tech. Discuss., https://doi.org/10.5194/amt-2018-79
Manuscript under review for journal Atmos. Meas. Tech.
Discussion started: 5 April 2018

Atmospheric Measurement Techniques
Open Access
Discussions

Table 3. Parameters of the Seventh-Order Polynomial Fits ($y=a_0+a_1x+a_2x^2+a_3x^3+a_4x^4+a_5x^5+a_6x^6+a_7x^7$) for λ = 1064 nm, with $x=\log(\beta_a)$ (in km^{-1} sr^{-1} unit) and $y=\log(\alpha_a, S_a, \text{or } V_a)$ in (km^{-1}, cm^2/cm^3 and cm^3/cm^3, respectively).

Functional relantionship at 355 nm	*Extinction coefficient*	*Surface area*	*Volume*
a_0	3.797837507651898	12.019452592845141	-5.314834128998254
a_1	3.294032541389781	30.825966279368547	2.500484347793244
a_2	0.962603336867675	24.518531616019207	-1.196109537503000
a_3	0.241796629870675	10.625241994796593	-1.583236058579546
a_4	0.064609145804688	2.634051072085453	-0.681801883947768
a_5	0.017721752150233	0.373150843707711	-0.145232662646142
a_6	0.002722551625862	0.027971628176431	-0.015471229968392
a_7	0.000157245409783	0.000854381337164	-0.000658925756875

Table 4. Mean Weighted LR at 355, 532 and 532 nm, derived in this work compared to the corresponding aerosol subtypes (clean continental, CC, and polluted continental, PC) from literature.

LR (sr)	*λ=355 nm*	*λ=532 nm*	*λ=1064 nm*
Omar et al., (2009) (Calipso aerosol model)	-	70 ± 25 (PC)	30 (PC)
	-	35 ± 16 (CC)	30 (CC)
Amiridis et al. (2015) (LIVAS database)	59.5* (PC)	64 (PC)	-
	56.5* (CC)	54 (CC)	-
Papagiannopoulos et al.. (2016) (EARLINET measurements)	-	62 ±10 (PC)	-
	-	47 ± 4 (CC)	-
Düsing et al.. (2018) (in-situ and lidar measurements)	55	55	30; 15**
This work	50.1 ± 17.9	49.6 ± 16.0	37.7 ± 12.6

* derived using the extinction-related and backscatter-related Ångström exponents given by Amiridis et al. (2013)

** see the explanation in the text for the two different values

Atmos. Meas. Tech. Discuss., https://doi.org/10.5194/amt-2018-79
Manuscript under review for journal Atmos. Meas. Tech.
Discussion started: 5 April 2018

Atmospheric Measurement Techniques
Discussions

Table 5. Main characteristics of the dataset of the EARLINET continental sites considered in this study. The listed dataset refer to the data downloaded from the EARLINET site (last access on the 11th of January 2018).

Station	*Number of points at 355 and at 532 nm)*	*Altitude* range (Δz, in km)	*Period*
Lecce (LC) 40.33 N, 18.10 E, 30 m a.s.l.	1012 – 109	1 – 4	Aug2007 – Oct2013
Leipzig *(LE)* 51.35 N, 12.43 E, 90 m a.s.l.,	5186 – 4549	1.5 – 4	Aug2008 – Sept2016
Potenza (PO) 40.6 N, 15.72 E, 760 m a.s.l.	1244 – 219	1.5 – 4	May2000 – Aug2009
Hamburg (HH) 53.57 N, 9.97 E, 25 m a.s.l.	243 – n.a.	0.5 – 4	Apr2001 – Oct2002
Madrid (MA) 40.45 N, 3.73 E, 669 m a.s.l.	n.a. – 492	0.5 – 4	Jun2006 – Jun2008

Atmos. Meas. Tech. Discuss., https://doi.org/10.5194/amt-2018-79
Manuscript under review for journal Atmos. Meas. Tech.
Discussion started: 5 April 2018

Atmospheric Measurement Techniques Discussions
Open Access

Table 6. Mean LR discrepancies between our model results and EARLINET measurements and mean (weighted) LR at 355 and 532 nm for the considered EARLINET stations.

	*[(LR$_{mod}$ - LR$_{meas}$)/LR$_{meas}$]*100*		*EARLINET weighted LR (sr)*	
Station	*λ=355 nm*	*λ=532 nm*	*λ=355 nm*	*λ=532 nm*
LC	10	18	51.8	44.5
LE	6	9	52.6	51.0
PO	17	7	44.9	57.2
HH	5	-	53.3	-
MA	-	6	-	54.2

Table 7. Main characteristics of the ALC and co-located sun-sky radiometer equipment located at the considered ALICENET sites.

	Site type	*ALC model*	*ALC firmware*	*Sun photometer model*
ASC	alpine	Nimbus CHM150104	0.743	POM-02
SPC	rural	Nimbus CHM110115	0.556	POM-02L
RTV	semi-rural	Nimbus CHM070052	0.720	CIMEL CE-318

Atmos. Meas. Tech. Discuss., https://doi.org/10.5194/amt-2018-79
Manuscript under review for journal Atmos. Meas. Tech.
Discussion started: 5 April 2018

Table 8. Results of the comparison between the AOT measured by sun-photometers and the one derived by ALCs (model-based and fixed LR inversion schemes) at three ALICENET stations. Mean differences (expressed in terms of <dAOT> = <(AOT_{ceil}-AOT_{phot})>, <|dAOT|> (module), <dAOT/AOT> and <|dAOTI/AOT|>) are reported with their standard deviations.

ALICENET sites	<dAOT>	<|dAOT|>	<dAOT/AOT>	<|dAOTI/AOT|>
ASC				
Variable LR from our model	-0.004 ± 0.015	0.010 ± 0.013	-0.25 ± 0.57	0.31 ± 0.35
LR = 52 sr	0.002 ± 0.021	0.009 ± 0.015	0.31 ± 0.58	0.33 ± 0.35
LR = 38 sr	-0.004 ± 0.014	0.009 ± 0.012	-0.23 ± 0.43	0.30 ± 0.32
SPC				
Variable LR from our model	-0.001 ± 0.020	0.013 ± 0.016	-0.005 ± 0.28	0.19 ± 0.20
LR= 52 sr	0.021 ± 0.026	0.026 ± 0.02	0.33 ± 0.35	0.38 ± 0.26
LR= 38 sr	-0.003 ± 0.019	0.011 ± 0.014	-0.043 ± 0.24	0.16 ± 0.18
RTV				
Variable LR from our model	0.004 ± 0.020	0.014 ± 0.014	0.11 ± 0.49	0.33 ± 0.30
LR= 52 sr	0.016 ± 0.023	0.021 ± 0.018	0.44 ± 0.59	0.49 ± 0.45
LR= 38 sr	0.003 ± 0.019	0.013 ± 0.013	0.088 ± 0.460	0.31 ± 0.27

Atmospheric Measurement Techniques Discussions
Open Access

Table 9. Extinction-to-volume conversion factors, $c_v = V_a/\alpha_a$ (and corresponding 'mass-to-extinctions efficiency' values, MEE $= \alpha_a/(V_a*\rho_a)$, given assuming $\rho_a = 2\ \mu g/m^3$) of continental particles as derived from our model at different wavelengths

Reference	*c_v [10^{-6}m] (corresponding MEE, [m^2g^{-1}])*			Notes
Wavelength [nm]	355	532	1064	
Hess et al. (1998)	-	0.35 (1.43)	-	OPAC, clean continental model
Hess et al. (1998)	-	0.28 (1.79)	-	Opac, polluted continental model
Barnaba and Gobbi (2004b)	-	0.18 (2.78)	-	Continental model
Ansmann et al. (2011b)	-	0.18 (2.78)	-	Germany, fine aerosol fraction
Lewandosky et al. (2010)	-	-	0.77 – 2 (0.25-0.65)	Mexico city basin
Sicard et al. (2012)	-	0.26 (1.92)	-	AERONET, Spain
Mamouri and Ansmann (2017)	0.17 (2.94)	0.30 (1.67)	0.96 (0.52)	Germany, continental anthropogenic pollution
Mamouri and Ansmann (2017)	0.23 (2.17)	0.41 (1.22)	1.41 (0.35)	Cyprus, continental anthropogenic pollution
Mamali et al. (2018)		0.14, 0.24 (3.57, 2.03)		Cyprus, fine non-dust aerosol fraction
This work	0.12 (4.17)	0.19 (2.63)	0.60 (0.83)	Continental (clean to moderately polluted)

Atmos. Meas. Tech. Discuss., https://doi.org/10.5194/amt-2018-79
Manuscript under review for journal Atmos. Meas. Tech.
Discussion started: 5 April 2018

Atmospheric Measurement Techniques Discussions

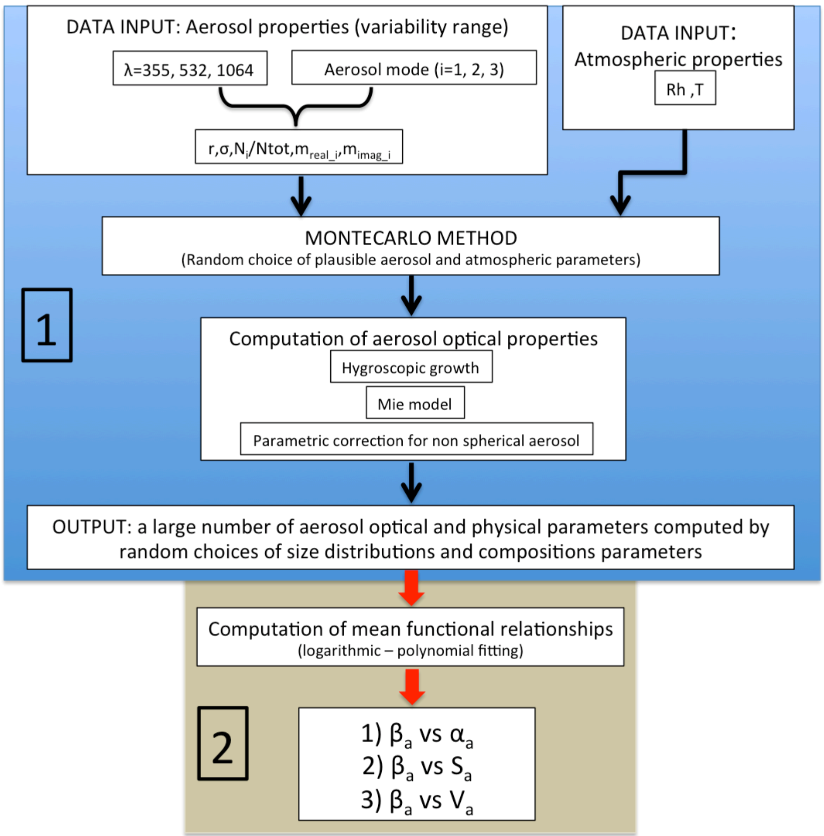

Figure 1. Schematic of the two-step model structure developed to obtain, as a result, functional relationships between the aerosol backscatter (β_a) and the aerosol extinction, surface area and volume (α_a, S_a and V_a, respectively).

Atmospheric Measurement Techniques Discussions
Open Access
EGU

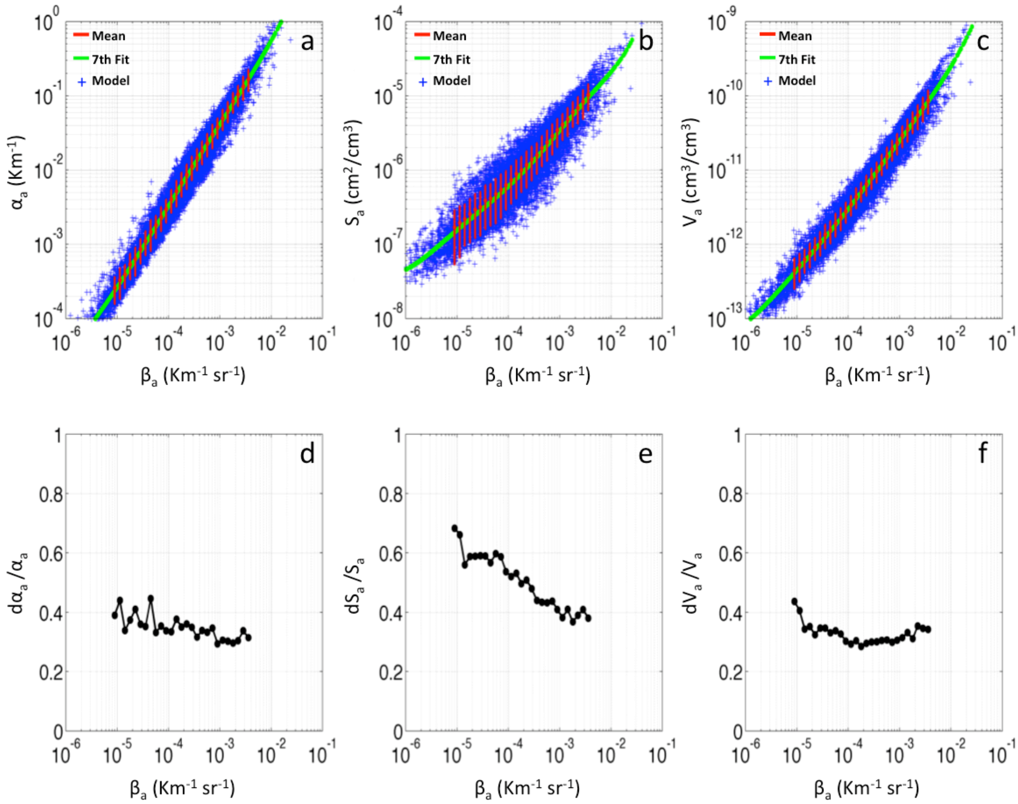

Figure 2. Scatterplots of a) α_a (km^{-1}), b) S_a (cm^2/cm^3) and c) V_a (cm^3/cm^3) vs backscatter ß$_a$ (km^{-1} sr^{-1}) and relevant relative errors (panels d, e, f, respectively) as derived from 20000 model computations (blue points) at λ = 1064 nm. Red dots and error bars are the average values per decade of ß and their standard deviations, green lines are the seventh-order polynomial fitting curve of the 20000 points.

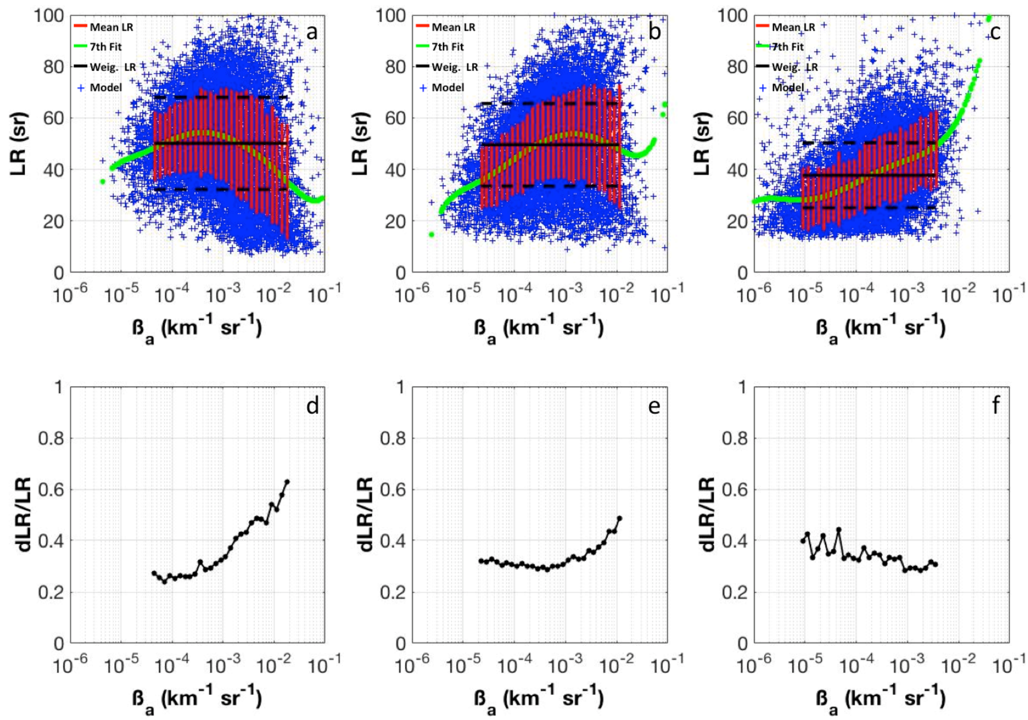

Figure 3. Upper plots: scatterplots of LR (sr) versus β_a (km^{-1} sr^{-1}) at: a) 355 nm; b) 532 nm; c) 1064 nm (blue points). The 7th-order polynomial fit curve (green lines) and the average values per decade of ß together with their standard deviations (red points and red vertical bars, respectively) are also reported. Horizontal black lines are mean values of the 'weighted-LR' and ± 1 s. d (solid and dotted lines, respectively). Lower plots: relative errors associated with the model-derived LR at d) 355 nm; e) 532 nm; f) 1064 nm.

Atmos. Meas. Tech. Discuss., https://doi.org/10.5194/amt-2018-79
Manuscript under review for journal Atmos. Meas. Tech.
Discussion started: 5 April 2018

Atmospheric Measurement Techniques
Discussions
Open Access

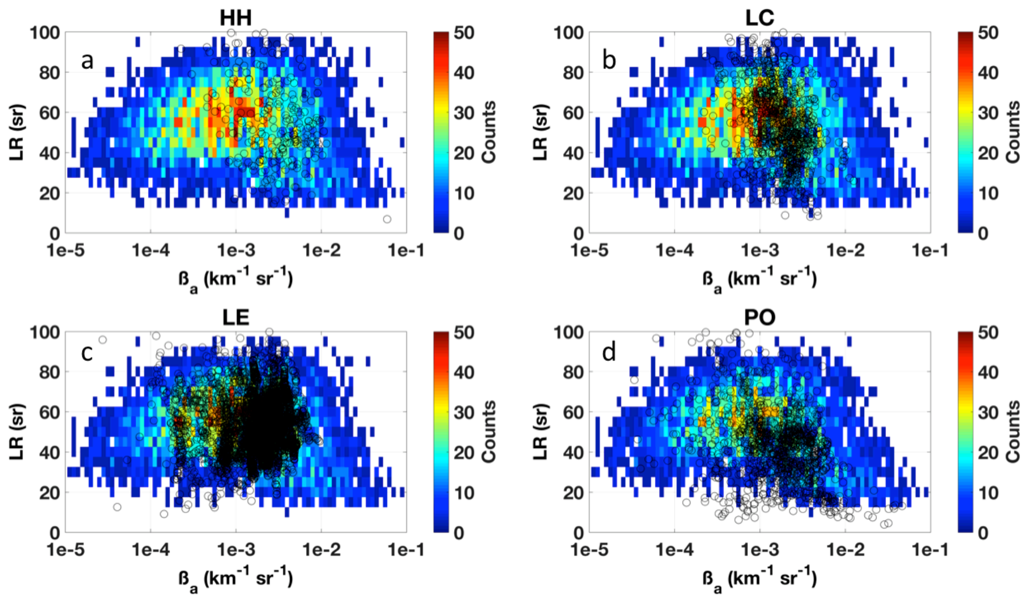

Figure 4. Scatterplots of LR (sr) versus ß$_a$ (km^{-1} sr^{-1}) at 355 nm as simulated by our model (colored region) and measured by EARLINET lidars (black open circles) in Hamburg (Germany) (a), Lecce (Italy) (b), Leipzig (Germany) c) and Potenza (Italy) (d). The color area is the region of simulated values, the color code indicating the number of simulated values in each ß$_a$ -LR pair (see legend). In particular, the color-2D histogram is computed using a semi-logarithmic box consisting of 10 equally spaced bins per decade of ß$_a$ in the x-axis and 5 spaced LR values in the y-axis.

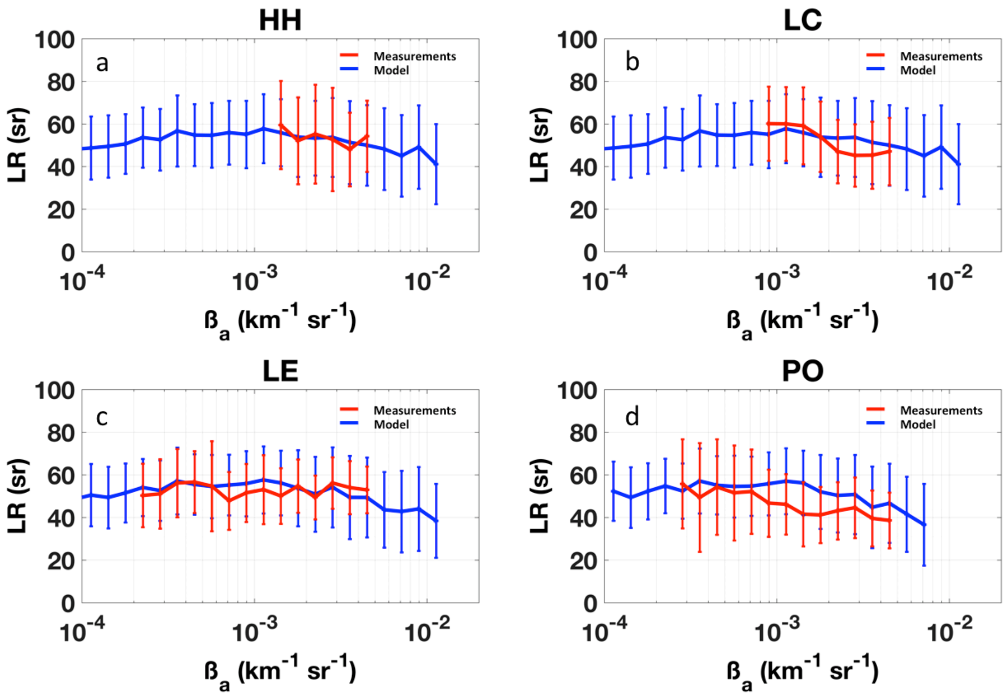

Figure 5. Model-simulated (blue) and lidar measured (red) LR vs $ß_a$ mean curves at 355 nm calculated per 10 equally spaced bins per decade of $ß_a$ in a) Hamburg, b) Lecce, c) Leipzig, and d) Potenza EARLINET lidar station. Vertical bars are the associated standard deviations.

Atmos. Meas. Tech. Discuss., https://doi.org/10.5194/amt-2018-79
Manuscript under review for journal Atmos. Meas. Tech.
Discussion started: 5 April 2018

Atmospheric Measurement Techniques
Discussions

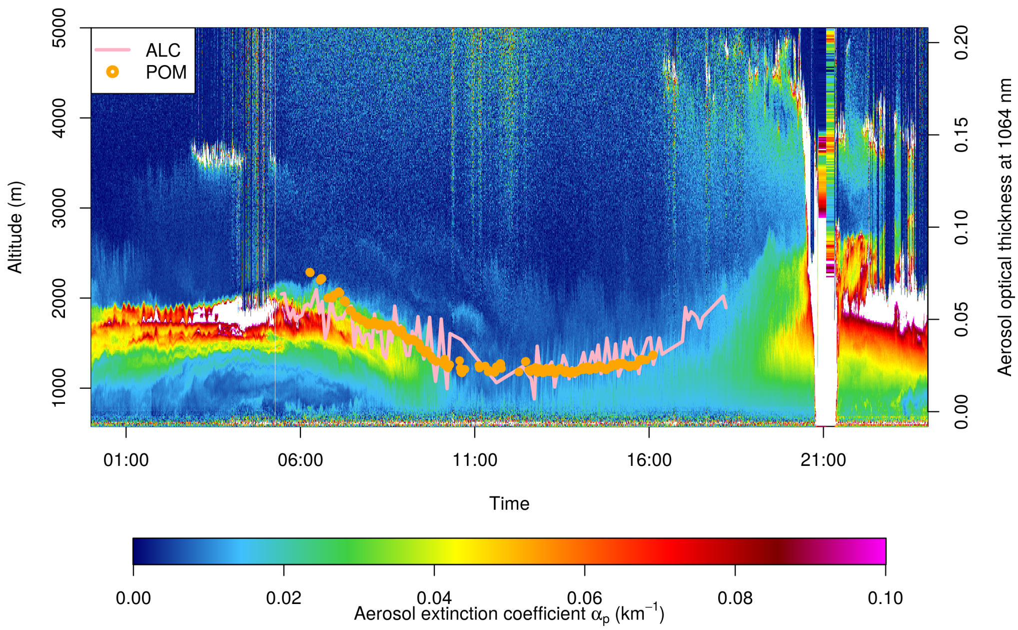

885

886 **Figure 6. Time-height cross-section of the aerosol extinction coefficients α_a [km^{-1}], as derived at 1064 nm on 26 June 2016 by**
887 **the ALICENET ALC of Aosta San Christophe (Northern Italy). The orange circle points and the pink line are the AOT**
888 **values (right y-axis, panel b) measured by a co-located POM-02L radiometer and estimated from the ALC following our**
889 **approach.**

890

Atmos. Meas. Tech. Discuss., https://doi.org/10.5194/amt-2018-79
Manuscript under review for journal Atmos. Meas. Tech.
Discussion started: 5 April 2018

Atmospheric Measurement Techniques
Open Access
Discussions

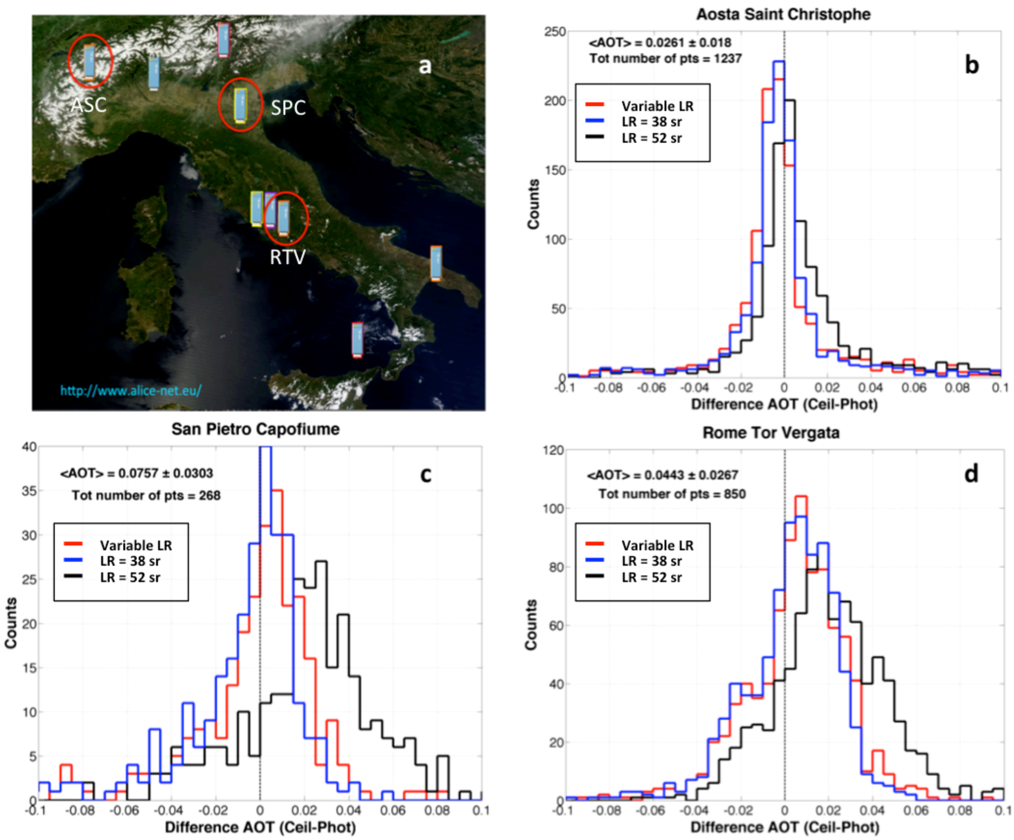

Figure 7. a) geographical map of the ALC network ALICENET. The red circles highlight the selected sites for this study: Aosta San Christophe (ASC), San Pietro Capofiume (SPC) and Rome Tor Vergata (ASC). b-d) histograms of the differences between the hourly-mean coincident AOTs at 1064 nm as derived by ALCs and measured by photometers, at ASC, SPC and RTV, respectively. The different colors (red, blue and black) depict the different inversion schemes: model-based inversion scheme, LR = 38 sr and LR = 52 sr, respectively. In each panel the values of the average measured AOT (and its associated standard deviation) and of the number of considered pairs are also reported.

Atmos. Meas. Tech. Discuss., https://doi.org/10.5194/amt-2018-79
Manuscript under review for journal Atmos. Meas. Tech.
Discussion started: 5 April 2018

Atmospheric Measurement Techniques
Open Access
Discussions

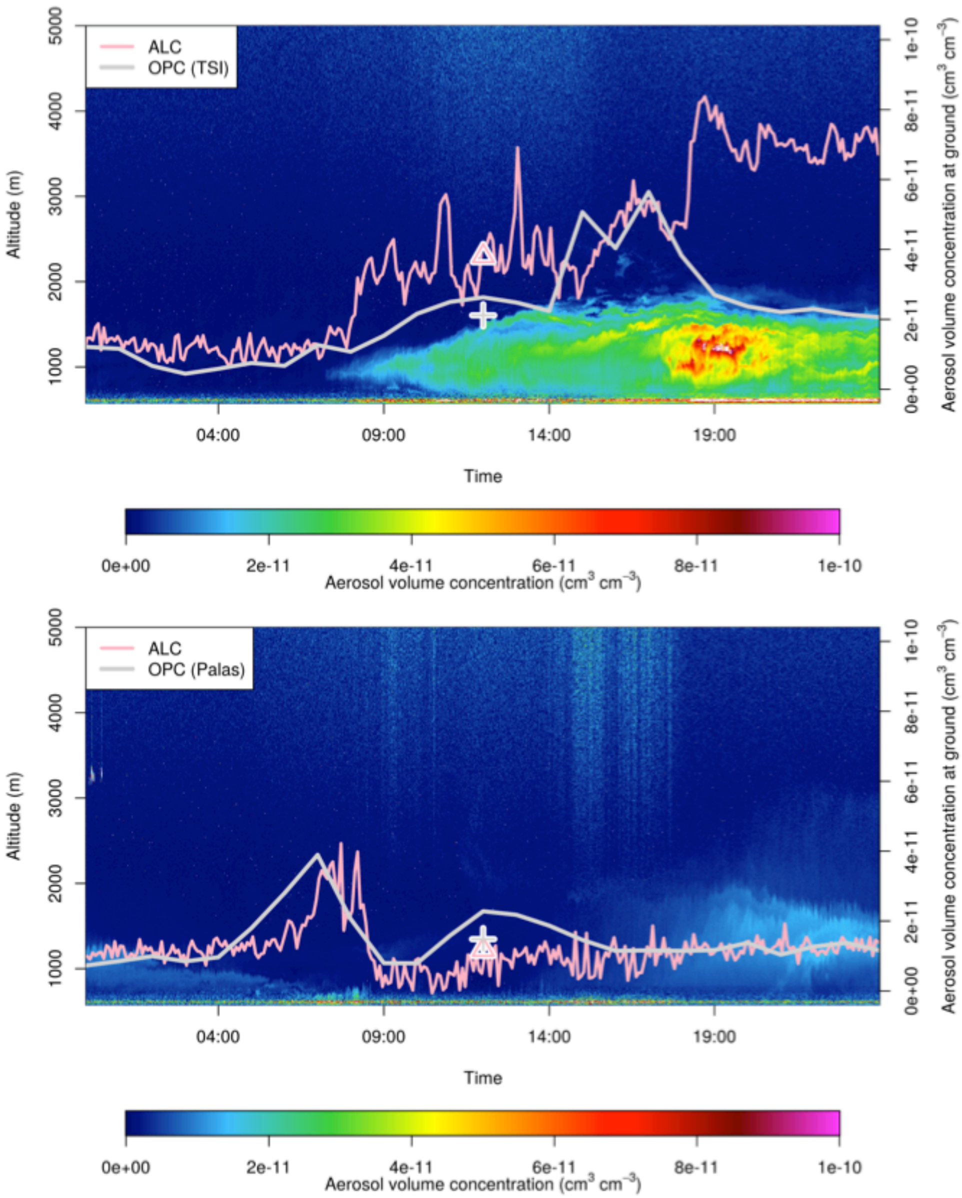

Figure 8. Time-height cross-section of the aerosol volume concentration at Aosta San Christophe for 29 December 2016 (upper panel) and 05 September 2017 (lower panel). The right y-axis reports the volume concentration measured at surface through TSI and Fidas®200s OPCs (upper and lower panels, grey curves) and the ALC-derived volume concentration at 75 m (pink curves). The grey crosses and the pink triangles refer to the daily mean aerosol volume value derived by OPCs and ALC measurements, respectively.

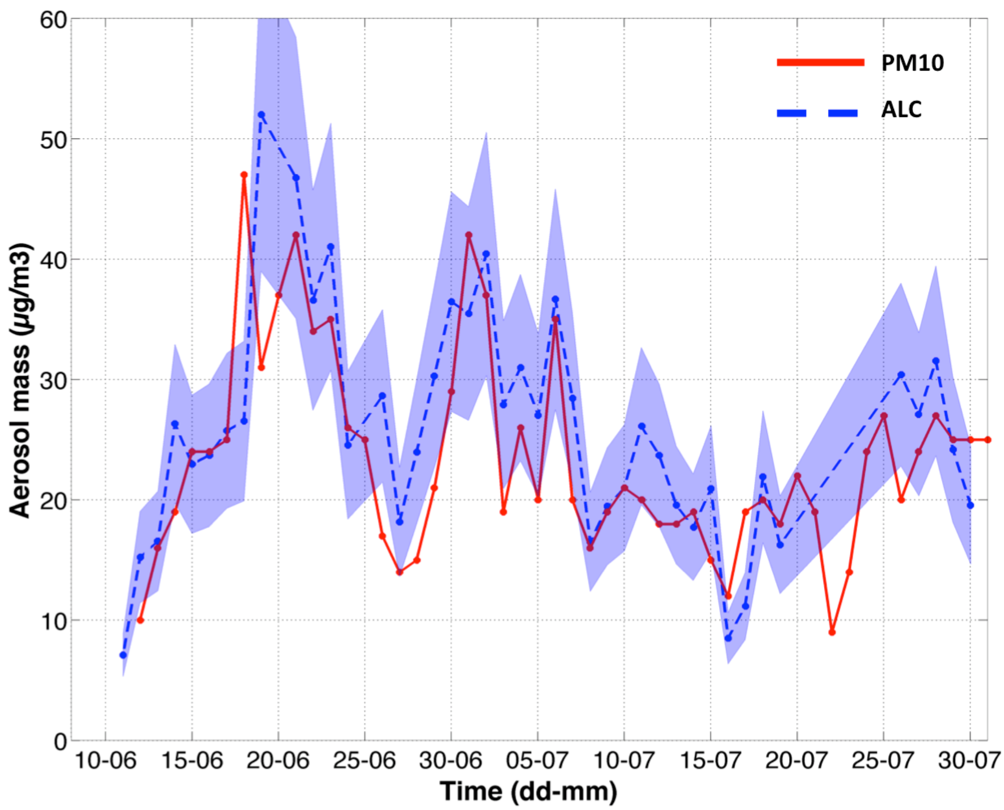

906

907 **Figure 9. Daily-resolved aerosol mass concentration at SPC, for the period June – July 2012, estimated from ALC-derived**
908 **aerosol volume data at 225 m a.s.l. converted into mass using a fixed particle density ρ_a = 2 μg/m^3 (blue dotted line) and a**
909 **variable ρ_a between 1.5 -2.5 μg/m^3 (shaded blue area). Red solid line are the daily PM10 concentration as measured by the**
910 **local Air Quality agency (ARPA).**

Atmos. Meas. Tech. Discuss., https://doi.org/10.5194/amt-2018-79
Manuscript under review for journal Atmos. Meas. Tech.
Discussion started: 5 April 2018

Atmospheric Measurement Techniques
Open Access
Discussions

Appendix A: Model-based functional relationships at 355 and 532 nm

The parameters of the seventh-order polynomial fit used to derive the functional relationships between log(x) and log(y) (where x = β_a and y =α_a, S_a or V_a) at λ = 355 and 532 nm are reported in Tab. A1 and Tab. A2, respectively.

Table A1. Parameters of the Seventh-Order Polynomial Fits ($y = a_0+ a_1x+a_2x^2+a_3x^3+a_4x^4+a_5x^5+a_6x^6+a_7x^7$) for λ = 355 nm, with x=log(β_a) (in km^{-1} sr^{-1} unit) and y=log(α_a, S_a, or V_a) in (km^{-1}, cm^2/cm^3 and cm^3/cm^3, respectively).

Functional relantionship at 355 nm	*Extinction coefficient*	*Surface area*	*Volume*
a_0	3.797837507651898	12.019452592845141	-5.314834128998254
a_1	3.294032541389781	30.825966279368547	2.500484347793244
a_2	0.962603336867675	24.518531616019207	-1.196109537503000
a_3	0.241796629870675	10.625241994796593	-1.583236058579546
a_4	0.064609145804688	2.634051072085453	-0.681801883947768
a_5	0.017721752150233	0.373150843707711	-0.145232662646142
a_6	0.002722551625862	0.027971628176431	-0.015471229968392
a_7	0.000157245409783	0.000854381337164	-0.000658925756875

Table A2. Parameters of the Seventh-Order Polynomial Fits ($y= a_0+ a_1x+a_2x^2+a_3x^3+a_4x^4+a_5x^5+a_6x^6+a_7x^7$) for λ = 532 nm, with $x=\log(ß_a)$ (in $km^{-1}\ sr^{-1}$ unit) and $y=\log(\alpha_a$, S_a, or $V_a)$ in (km^{-1}, cm^2/cm^3 and cm^3/cm^3, respectively).

Functional relantionship at 532 nm	*Extinction coefficient*	*Surface area*	*Volume*
a_0	3.797837507651898	12.019452592845141	-5.314834128998254
a_1	3.294032541389781	30.825966279368547	2.500484347793244
a_2	0.962603336867675	24.518531616019207	-1.196109537503000
a_3	0.241796629870675	10.625241994796593	-1.583236058579546
a_4	0.064609145804688	2.634051072085453	-0.681801883947768
a_5	0.017721752150233	0.373150843707711	-0.145232662646142
a_6	0.002722551625862	0.027971628176431	-0.015471229968392
a_7	0.000157245409783	0.000854381337164	-0.000658925756875

Atmos. Meas. Tech. Discuss., https://doi.org/10.5194/amt-2018-79
Manuscript under review for journal Atmos. Meas. Tech.
Discussion started: 5 April 2018

Atmospheric Measurement Techniques
Discussions
Open Access

Appendix B: Model sensitivity tests

To evaluate the proposed continental model configuration (hereafter CM0) and discuss its sensitivity to the variability of the employed parameters, an overview of the impact on the model results produced by changing the limit of the variability ranges of these parameters (i.e. using different model configuration, CMX) is given in this section.

The varied model (CMX-CM0) mean difference on the considered optical property (OP) has been quantified through the following equation:

$$< \frac{dOP}{OP} > = \left(\frac{1}{Nbin}\right) \cdot \sum_{i=1}^{Nbin} [(< OP_{CMX} >_i - < OP_{CM0} >_i) / < OP_{CM0} >_i], \qquad \text{(A.1)}$$

where N_{bin} is the total number of defined bins of β_a.

The results of the mean differences of α_a and LR for different ranges of β_a and for the whole β_a interval are reported on table A1, where relevant sensitivity cases (i.e. relative mean difference greater than 1%) at λ=355 nm have been taken into account.

CM1 refers to a model configuration without the first aerosol mode (N_1%=0). The overall decrease on the values of α_a and LR (around 3-4%) is due to the sum of significant and opposite effects for low and high values of β_a where $<d\alpha_a/\alpha_a>$ and $<dLR/LR>$ are of the order of -6% and 8%, respectively. Removing the coarser aerosol mode (N_3%=0), causes positive mean values for $<d\alpha_a/\alpha_a>$ and $<dLR/LR>$ of the order of 5% (sensitivity case CM2). In this case, the largest impact is observed for the β_a range between 2×10^{-4} and 2×10^{-3} km^{-1}sr^{-1}.

An opposite result is obtained by decreasing the upper bound of the r_2 variability range (r_2=0.03 – 0.05 µm, CM3). In fact also this model configuration leads to lower α_a and LR ($<d\alpha_a/\alpha_a>$ and $<dLR/LR>$ are equal to -6%, approximately). In this case, the variation on the r_2 parameter affects the higher ranges of β_a ($\beta_a=2\times10^{-4}$-2×10^{-2} km^{-1}sr^{-1}). Higher modal radii for the coarse-mode particle (r_3=1 – 1.2 µm) in CM4 configuration leads to the increase of the contribution of model-generated points with higher β_a and causes lower values of α_a and LR ($<d\alpha_a/\alpha_a>$ and $<dLR/LR>$ are equal to -5%, approximately) only for high values of β_a ($\beta_a=2\times10^{-3}$-2×10^{-2} km^{-1}sr^{-1}), whereas the effect over the whole β_a range is around -1%.

The CM5 configuration accounts for the presence of more absorbing particles in the first aerosol mode, where the lower bound of m_{1im} has been increased by a factor of 10 (m_{1im} =0.1-0.47). This produces a significant effect only for the lower values of β_a ($\beta_a=2\times10^{-5}$-2×10^{-4} km^{-1}sr^{-1}), with an increase of α_a and LR of approximately 4%. On the contrary, increasing the lower bound of the real part of the second aerosol mode refractive index (m_{2r} =1.55-1.70) has a large impact on the considered parameters. In fact, the CM6 configuration largely underestimates both α_a and LR (around -15% for both parameters) for all β_a ranges.

The CM7 configuration refers to the impact of the total number of particles at the ground (N_{tot}). In this case, decreasing the upper bound of the variability range of N_{tot} by a factor of 2 (N_{tot} =500-5000 cm^{-3}) lowers the mean values of α_a and LR of around 5%. Nevertheless, this effect is totally due to the contribution of the β_a values between 2×10^{-3} and 2×10^{-2} km^{-1}sr^{-1}, where $<d\alpha_a/\alpha_a>$ and $<dLR/LR>$ are around -10%. Assuming no increase with altitude for $\sigma_{1,2}$ (sensitivity case CM8) produces relevant differences on the mean values of α_a and LR. In CM8, the overall overestimation of these two parameters is quite limited ($<d\alpha_a/\alpha_a>$ = 6.3 and $<dLR/LR>$ =6.4), whereas a large and opposite impact is observed for

Atmos. Meas. Tech. Discuss., https://doi.org/10.5194/amt-2018-79
Manuscript under review for journal Atmos. Meas. Tech.
Discussion started: 5 April 2018

low and high values of β_a. In fact, $<d\alpha_a/\alpha_a>$ ($<dLR/LR>$) is equal to -14.1 (-13.9) and 18.5 (19.0) for β_a= 2×10^{-5} - 2×10^{-4} and β_a= 2×10^{-5} - 2×10^{-4} $km^{-1}sr^{-1}$, respectively. As explained by Barnaba et al. (2007), the dependence of $\sigma_{1,2}$ to the altitude can be associated to the fact that, when increasing the distance from the main aerosol sources, the particle processing is more efficient.

Table B1. Mean differences of α_a and LR between different model sensitivity cases and the proposed continental model configuration.

Model configuration	β_a ($km^{-1}sr^{-1}$) 2×10^{-5}-2×10^{-4}		β_a ($km^{-1}sr^{-1}$) 2×10^{-4}-2×10^{-3}		β_a ($km^{-1}sr^{-1}$) 2×10^{-3}-2×10^{-2}		β_a ($km^{-1}sr^{-1}$) 2×10^{-5}-2×10^{-2}	
	$<d\alpha_a/\alpha_a>$ (%)	$<dLR/LR>$ (%)	$<d\alpha_a/\alpha_a>$ (%)	$<dLR/LR>$ (%)	$<d\alpha_a/\alpha_a>$ (%)	$<dLR/LR>$ (%)	$<d\alpha_a/\alpha_a>$ (%)	$<dLR/LR>$ (%)
CM1 (N_1%=0)	-6.2	-6.4	3.1	3.2	7.8	7.9	-3.7	-3.5
CM2 (N_3%=0)	4.7	4.9	8.6	8.9	2.8	2.7	5.3	5.4
CM3 (r_2=0.03 – 0.05 µm)	-2.0	-1.7	-10.3	-10.2	-8.9	-8.2	-6.7	-6.4
CM4 (r_3=1.0 – 1.2 µm)	<1	<1	-2.1	-2.0	-5.24	-5.3	-1.2	-1.0
CM5 (m_{1im}=0.1-0.47)	4.3	4.2	<1	<1	<1	<1	1.8	1.8
CM6 (m_{2r}=1.55 – 1.70)	-10.9	-10.9	-16.2	-16.3	-18.9	-19.1	-15.3	-15.3
CM7 (N_{TOT}=500-5000)	<1	<1	<1	<1	-11.2	-10.7	-3.7	-3.5
CM8 (σ_1, σ_2 constant)	-14.1	-13.9	6.4	6.1	18.5	19.0	6.3	6.4

Atmos. Meas. Tech. Discuss., https://doi.org/10.5194/amt-2018-79
Manuscript under review for journal Atmos. Meas. Tech.
Discussion started: 5 April 2018

Atmospheric Measurement Techniques
Open Access
Discussions

Appendix C: Model – EARLINET comparison at 532 nm

Figure C1 depicts the result of the comparison between EARLINET stations and our developed model (red and blue curves, respectively) in terms of 'mean' LR per bin of $ß_a$ at λ=532 nm. Note that only $ß_a$ bins containing at least 1% of the total modeled data were considered. Similarly to the results at 355 nm shown in section 4.1, a general good agreement between the modeled and the measured LR values is found. As attested by the low value of the mean discrepancy of Table 6, the modeled curve well fits with Madrid observations. Some major deviations are found for Lecce, which, however, at 532 nm, has a very low number of considered points (i.e. 109).

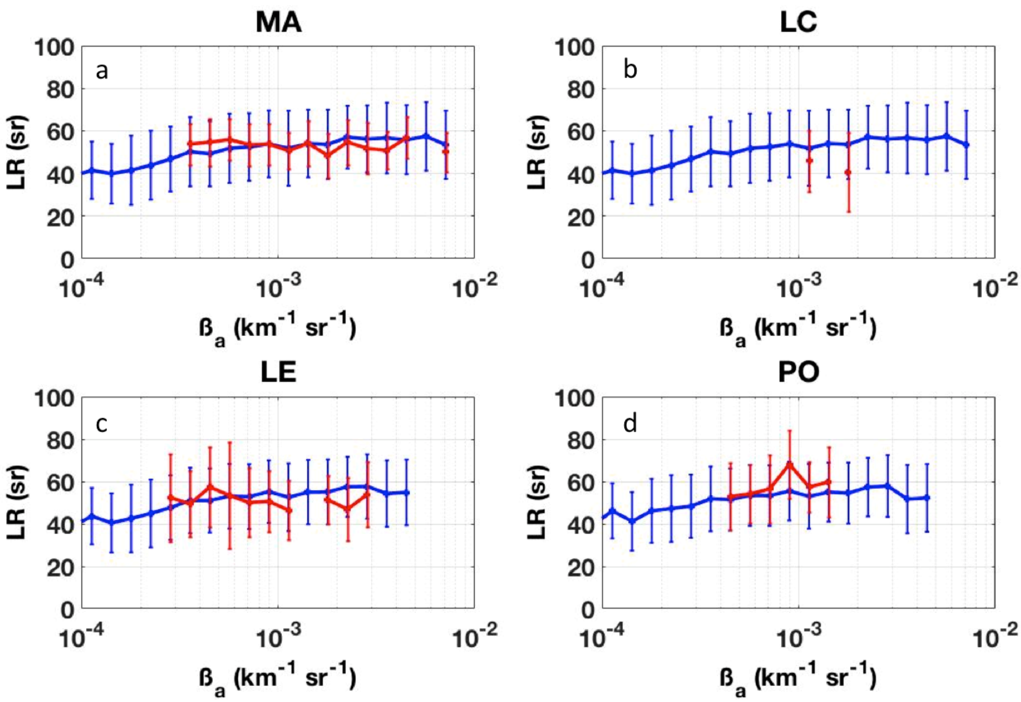

Figure C1. Model-simulated (blue) and lidar measured (red) LR vs ßa mean curves at 532 nm calculated per 10 equally spaced bins per decade of ßa in a) Madrid, b) Lecce, c) Leipzig, and d) Potenza EARLINET lidar station. Vertical bars are the associated standard deviations.

Atmos. Meas. Tech. Discuss., https://doi.org/10.5194/amt-2018-79
Manuscript under review for journal Atmos. Meas. Tech.
Discussion started: 5 April 2018

Atmospheric Measurement Techniques
Discussions

Appendix D: Model sensitivity tests for optimal configurations at LC and PO sites

According to the results reported in Tab. B1, two model configurations (CM0a and CM0b) have been set up to better reproduce the EARLINET observations of LR vs β_a at LC and PO sites, respectively. The comparison between these two configurations, the EARLINET measurements and the CM0 set-up are illustrated in Fig. B1 (panel a and b for LC and PO, respectively) in terms of LR mean value curves per 10 equally spaced bins per decade of $ß_a$. Blue and red colors have the same meaning of Fig. 5 (i.e. CM0 model and observation curves, respectively), black curves refer to the LR vs β_a estimated through the CM0a and CM0b model versions for LC and PO stations, respectively. Vertical bars are the associated standard deviations.

The only difference between CM0a and CM0 configuration consists in the upper bound of the variability range of N_{tot} (5000 vs 10000 cm^{-3} at ground, respectively). This modification seems to fit the observed LR vs β_a behavior at 355 nm. The upper bound N_{tot} value is similar to the one (i.e. N_{tot} upper bound =3000 cm^{-3} at ground) used in the work of Barnaba et al. (2007) to characterize the optical properties of the continental aerosol present over southeastern Italy. The computed mean model-measurement LR relative difference between CM0a configuration and LC Earlinet measurements is around 5%.

Similarly, the CM0b configuration uses the same value for the upper bound of N_{tot} variability range and, in addition, higher values of the r_3 variability range of (1.0 – 1.2 µm vs 0.3 - 0.5 µm, respectively). As highlighted by the panel b of Fig. B1, this model configuration allows well reproducing the LR vs β_a behavior derived by EARLINET lidar Raman measurements at 355 nm. This result seems to indicate the presence of coarser aerosols in a clean continental environment. In comparison to the CM0 model, the mean model-measurement LR relative difference decreases from 17% to 6%.

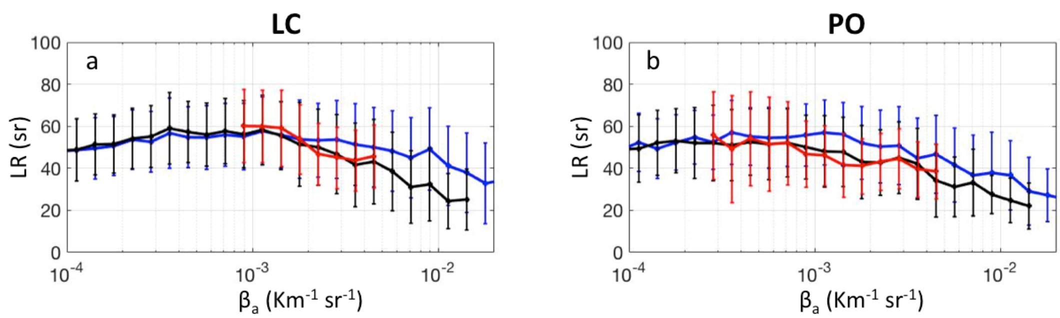

Figure D1. Model-simulated (blue and black lines) and lidar measured (red lines) LR vs $ß_a$ mean curves at 355 nm calculated per 10 equally spaced bins per decade of $ß_a$ for the LC and PO EARLINET lidar stations (panel a and b, respectively). Blue color refers to CM0 model configuration, black color to CM0a and CM0b model configurations adapted to LC and PO sites, respectively.